GEOLOGY OF THE MARYSVILLE MINING DISTRICT, MONTANA:

TWO PHASES OF MINERALIZATION

by

Evan Charles Gearity

A thesis submitted in partial fulfillment
of the requirements for the degree

of

Master of Science

in

Earth Science

MONTANA STATE UNIVERSITY
Bozeman, Montana

July 2013

APPROVAL

of a thesis submitted by

Evan Charles Gearity

This thesis has been read by each member of the thesis committee and has been found to be satisfactory regarding content, English usage, format, citation, bibliographic style, and consistency, and is ready for submission to The Graduate School.

Dr. Colin Shaw

Approved for the Department of Earth Science

Dr. David Mogk

Approved for The Graduate School

Dr. Ronald W. Larsen

STATEMENT OF PERMISSION TO USE

In presenting this thesis in partial fulfillment of the requirements for a master's degree at Montana State University, I agree that the Library shall make it available to borrowers under rules of the Library.

If I have indicated my intention to copyright this thesis by including a copyright notice page, copying is allowable only for scholarly purposes, consistent with "fair use" as prescribed in the U.S. Copyright Law. Requests for permission for extended quotation from or reproduction of this thesis in whole or in parts may be granted only by the copyright holder.

Evan Charles Gearity

July 2013

TABLE OF CONTENTS

TABLE OF CONTENTS - CONTINUED

LIST OF TABLES

LIST OF FIGURES

Figure Page

LIST OF FIGURES - CONTINUED

Figure Page

ABSTRACT

The Lewis & Clark line extending from Idaho to Eastern Montana is known for its numerous mineral deposits. Recent advances in our understanding of regional tectonics, the geological history of the Lewis and Clark line, and how mineral deposits form, provide an opportunity for a deeper investigation into this previously studied region. The Marysville Mining District (MMD) is located in the Lewis & Clark line and was chosen for this study. Renewed interest in the MMD allowed for access to the Drumlummon gold mine and the Bald Butte molybdenite deposit. This study applied recent advances in regional tectonics, knowledge of mineral deposit formation, age dating, and geochemical techniques, providing new insights into the MMD with an emphasis on the Drumlummon gold mine. The methods used to conduct this study included field mapping, geochronology, FEM-EDS, and computer-based paleostress reconstruction. Results from this investigation were combined with previous work done to form ideas on the origins of mineral deposits in the MMD and the roles of regional tectonics on the emplacement of mineralized veins. The new age dates in the MMD reveal that mineralization occurred in two events: at ~80 Ma and ~40 Ma. Mapping results showed a deformation history in the MMD that included the transpression and transtension events experienced on the Lewis & Clark line. The mineralized veins at the Drumlummon gold mine and Bald Butte molybdenite prospect tend to follow the transtensional stress field. The ore mineralogy of the Drumlummon gold mine is most consistent with an intermediate sulfide epithermal system. Using the new data, a hypothesis was proposed that the origin of gold in the Drumlummon mine was the Silver City Stock.

INTRODUCTION AND TECTONIC SETTING

This project sets out to apply recent knowledge in economic geology and regional tectonics to further the understanding of previously discovered metal deposits in the west-central Montana segment of the Lewis & Clark line (LCL). The LCL is an 800 km long and 40-80 km wide major transverse structure (Faulds & Varga, 1998) that extends southeastward from eastern Washington to east of Helena, Montana (Figure 1). The LCL accommodated complex oblique deformation during both Late Cretaceous-Late Paleocene contraction and Tertiary extension in the northern Rocky Mountain region (Sears & Hendrix, 2004, Sears et al., 1998, Lageson & Stickney, 2000). Subduction of the Pacific plate under North America was also occurring during the deformational episodes, producing widespread magmatism and plutonism across the western United States. Major subduction-related metal deposits associated with the Cretaceous-Tertiary plutons occur throughout the region predominantly concentrated in several belts. The Idaho-Montana porphyry belt is one such belt that is partly coincident with the west-central Montana portion of the LCL (Armstrong, Hollister, & Harakel, 1978, Rostad, 1978). This segment of the porphyry belt provides an opportunity to study the interaction between transcurrent tectonic deformation and subduction-related intrusive deposits. Other studies have also suggested a link between regional tectonic controls and the mineralization style of subduction-related deposits (Tosdal & Richards, 2001).

The Marysville Mining District (MMD) (Figure 1) was chosen as the study area for this thesis because of its location in both the LCL and Idaho-Montana porphyry belt and because of the recent revival of interest in the economic potential of the district. Metal deposits in the MMD include base metal (Bald Butte molybdenum prospect) and precious metal deposits (Drumlummon and many other gold mines). The goals of this thesis are to: (1) produce a deposit model for the Drumlummon gold mine in the MMD, (2) explain controls on the emplacement of ore veins at the Drumlummon gold mine and Bald Butte, (3) establish the timing of mineralization in the MMD, and (4) investigate the effects of transpression and transtension on local structures in the LCL.

Regional Tectonic Setting

Tectonic events in southwest Montana since Jurassic time can be divided into four major episodes with the tectonic setting starting with shortening and transitioning into extension. Shortening initiated with the Sevier Orogeny during the Late Jurassic subduction of the Farallon plate along the western margins of North America (Dickinson, 2004, DeCelles, 2004) and is characterized by a series of westward dipping thrust sheets. The thrust sheets formed a thin-skinned fold-and-thrust belt that imbricated the sedimentary wedge thrusting it eastward towards the North American craton (Figure 1) (Armstrong, 1968). This tectonic wedge of sedimentary rocks was thrust further east in southwest Montana forming the Helena salient which is bounded to the north by the LCL (Figure 1). Shortening

related to the Sevier Orogeny continued into Late Cretaceous time (Kalakay, John & Lageson, 2001), overlapping with deformation styles related to Laramide Orogeny (Figure 2). The Laramide orogeny is characterized by thick-skinned deformation involving uplifted basement blocks (Kulik & Schmidt, 1988). Typical Laramide-style deformation dominates the mountains of Wyoming, Colorado, and southwestern and west-central Montana. During both the Sevier and Laramide orogenies subduction of the Farallon plate caused partial-melting of the overriding North American plate and mantle wedge creating a magma source (Figure 3) (Foster et al., 2001, Hyndman, 1981).

Two phases of extension followed the Laramide orogeny in southwest Montana. The first phase is the extensional collapse of the Cordilleran fold-and-thrust belt beginning around 50 Ma and transitioning into Basin and Range style extension after roughly 20 Ma (Figure 2) (McCay, 1978, Lageson & Stickney, 2000). The extensional collapse of the fold-and-thrust belt is characterized by metamorphic core complex development, rifting, and basin development (Janecke, Vandenburg, & Blankenau, 1998, Janecke & Blankenau, 2003). Both the ~50 Ma age and characteristic styles for extensional collapse of the Cordilleran fold-and-thrust belt are observed in the Helena salient (Figure 2) (O'Neill et al., 2004, Hodges & Applegate, 1993, House, Bowring, & Hodges, 2002). The extensional collapse of the orogenic wedge in southwest Montana transitioned into Basin and Range extension around 20 Ma (Constenius, 1996) as deformational styles related to the Cordilleran fold-and-thrust belt gave way to widespread extensional block faulting. Basin and

Range style extension began in southwestern North America at about 35 Ma and gradually progressed northwards as the Mendocino triple junction migrated along the western North American plate margin (Atwater, 1970). Basin and Range style extension is observed in southwest Montana starting at roughly 20 Ma. Although better known in the Great Basin of Nevada and western Utah, the Basin and Range extensional province continues at least to the north end of the Flathead Valley in northern Montana based on structural morphology and Intermountain Seismic Belt seismicity (Lageson & Stickney, 2000). Previous workers have estimated the maximum Basin and Range extension in Montana at ~25 km (McMechan & Price, 1984, Harrison & Bally, 1988), while others have argued that the total extension may be greater than ~30 km based on large displacements on listric normal faults (Constenius, 1996). Two hypotheses have been proposed as the cause of the tectonic transition from shortening to extension: (1) a rapid drop in the rate of convergence between the North American plate and the subducting Farallon plate, and (2) a steepening of the subduction angle of the subducting Farallon plate (Constenius, 1996, Coney & Reynolds, 1977, Ward, 1995, Wernicke, 1992). In either case, the relaxation of end-loading tectonic forces is thought to have facilitated the gravitational collapse of the orogenic wedge on extensional listric normal faults that sole into regional detachment faults (Smithson & Johnson, 1989, Foster et al., 2007).

Lewis and Clark Line

The LCL is a persistent transverse structure with a complex history of reactivation in response to evolving tectonic conditions. The LCL initiated as a rift structure during the Mesoproterozoic opening of the Belt Basin between 1500 and 1370 Ma (Sears, MacDonald, & Lonn, 2010, Ross, Parrish, & Winston, 1992). The Belt Supergroup, a >15km thick sequence of sedimentary rocks, was deposited during this time (Figure 4) (Ross & Villeneuve, 2003, Evans et al., 2000, Ross, Skipp, & Rezak, 1963). The LCL was reactivated during the Cretaceous-Late Paleocene Sevier and Laramide orogenies when it accommodated differential shortening along the northern margin of the Helena salient in the overthrust belt (Wallace, Lidke, & Schmidt, 1990) causing sinistral transpression in the LCL (Figure 3) (Sears & Hendrix, 2004). Sinistral transpression on the LCL transitioned to dextral transtension starting at ~50 Ma during the extensional collapse of the Cordilleran fold-and-thrust belt (Foster et al., 2007) (Figure 3). Regional structures in the LCL related to transpression and transtension have a northwest-southeast orientation (Sears et al., 2010, Wallace et al., 1990). The applied transpressive and transtensive shear stresses on the LCL favored the development of localized extensional faults that act as conduits focusing magma emplacement and related porphyry mineralization (Tosdal & Richards, 2001).

The LCL has 10 principal faults, each having 11 to 28 km of complex strike-slip, dip-slip, and oblique-slip offset (Figure 5) (Wallace et al., 1990). The MMD is located within the two easternmost principal faults of the LCL: the Bald Butte fault

to the west and the St. Marys-Helena Valley fault to the east (Figure 5). The St. Marys-Helena Valley fault experienced 13 km of right lateral offset that occurred principally between Late Cretaceous and Early Eocene times (Wallace et al., 1990). The Bald Butte fault experienced up to 28 km of right lateral offset and was active from 97 to 47-44 Ma (Wallace et al., 1990). Only minor movement on the Bald Butte fault has been documented after 44 Ma. The right lateral movement on the Bald Butte and St. Marys-Helena Valley faults during the Late Cretaceous-Late Paleocene is consistent with the sinistral transpression model postulated by Sears and Hendrix (2004).

Wallace et al. (1990) stated that the zone of convergence between the St. Marys-Helena Valley and Bald Butte principal faults has four distinct structural styles characterizing different tectonic events. The first two structural styles consist of local thrust faults and northwest-striking, northeast-dipping reverse faults that record contraction produced by right lateral movement along the LCL principal faults. Some of these faults predate late Cretaceous stocks. The third structural style related to shortening consists of northwest-striking folds parallel to northwest reverse faults, some of which are late Cretaceous in age. All three of these structural styles are consistent with the existence of a sinistral transpressional system along the LCL with antithetic dextral faults accommodating block rotation (Figure 3) during the late Cretaceous. The fourth structural style occurs at a double bend along the Bald Butte Fault ~20 km northwest of Helena. In this area, a fault wedge south of the restraining bend is down-dropped relative to rocks north of the restraining bend

as would be predicted in a right-slip system. The fourth structural style is outside the mapping area selected for this thesis.

The Marysville Mining District

The Marysville Mining District (Figure 1) provides a study area which has been hypothesized to have undergone both Late Cretaceous-Late Paleocene transpression and Tertiary transtension. Previous structural deformation was largely confined to the Proterozoic (Ross et al., 1963). The MMD has one known intrusive event during Late Cretaceous-Late Paleocene transpression and three known intrusive events during Tertiary transtension (Walker, 1992a). Some of the Tertiary intrusions in the MMD are known sources of mineralization (Walker, 1992). Intrusive-related metamorphism and alteration in the MMD overprint a low grade Proterozoic regional metamorphism that affected the Belt Supergroup country rocks (Ross et al., 1963, Petefish, 1975). The renewed mining activity in the MMD with the recent rise in metal prices allowed access to some underground workings in the Drumlummon Gold Mine. Access to the underground workings allowed detailed observations of structural relationships.

Rock Types

Belt Supergroup (Country Rocks)

Empire Formation: The Empire Formation is a shale-rich unit in the Belt Supergroup (Figure 4). The formation is a thin-bedded, dense, calcareous to dolomitic, siliceous shale or argillite. It has a light to dark greenish-gray color (Ross

et al., 1963) and may be a light to dark brown thin-bedded shale in its lower parts (Petefish, 1975). When metamorphosed the formation changes to a very light to dark green or black, banded to non-banded, fine-grained hornfels (Petefish, 1975). The Empire Formation has been observed up to 205 meters thick in the MMD (Blackwell et al., 1974).

Helena Formation: The Helena Formation is a carbonate unit that overlies the Empire Formation in the Belt Supergroup (Figure 4). The Helena Formation consists of thick-bedded, bluish-gray to gray limestone and black to buff, weathered dolostone. Gray, green, red, and purplish shale may be found in beds up to a few meters thick (Ross et al., 1963). Knopf (1950) found siliceous oolites, edgewise conglomerates, and stromatolites in the Formation. Petefish (1975) found cross-bedded, silty shales up to 0.3-0.6 meters thick in the Formation. The impure limestone and dolostone generally become a coarser-grained, often banded, white to light green to brown hornfels with increasing metamorphism. The light-green (diopside and/or actinolite) and brown (phlogopite) colorations are in locations where dolomite, quartz, and calcite in the original sediments have reacted (Petefish, 1975). The maximum thickness of the Helena Formation in the MMD was estimated to be up to ~1200 meters (Barrell, 1907).

Cretaceous Intrusives

Marysville Stock

The Marysville stock is a prominent feature located in the middle of the MMD outcropping over roughly 8.3 square kilometers (Figure 6). The Marysville stock is of granodiorite composition and has been age-dated at 78±4 Ma using the $^{40}K/^{40}Ar$ method (Baagsgaard, Folinsbee, & Lipson, 1961a). The Marysville stock was hypothesized as having been emplaced by magma stoping by Barrell (1907). Fluid inclusion work done by Petefish (1975) estimated the emplacement depth of the currently exposed Marysville stock at 4 ± 1 km.

Eocene Intrusives

Silver City Stock

The Silver City stock is located 8 miles east-southeast of the Marysville stock and outcrops over roughly 2.8 kilometers (Figure 6). The Silver City stock is a biotite andesite-dacite porphyry and has been age-dated at 43.2±2.6 Ma using the $^{40}K/^{40}Ar$ method (Petefish, 1975).

Bald Butte Intrusive

The Bald Butte intrusive is a "blind" pluton located ~1.5 miles southwest of the Marysville stock and has a 38.6±1.5 Ma date using $^{40}K/^{40}Ar$ by Gulf Minerals Resources Co. in 1978. In surface outcrop, only the alteration related to the unexposed intrusive is observed. The extent of the intrusive in the subsurface is delineated by drill core (Walker, 1992a). Compositionally, the Bald Butte intrusive is

a leucocratic quartz porphyry with quartz eyes and feldspar phenocrysts in a fine-grained ground mass. Locally, a zone of silica alteration is found above the main intrusive body. Based on fluid inclusion work, Petefish (1975) estimated the emplacement depth of the Bald Butte intrusive at 2.3 km.

Empire Creek Intrusive

The Empire Creek intrusive is a quartz-feldspar (granite) porphyry and is overlain by massive silica similar to the Bald Butte intrusive (Walker, 1992b). The Empire Creek intrusive was dated at ~40 Ma (Walker, 1992b). Based on fluid inclusion work, Petefish (1975) estimated the emplacement depth of the Empire Creek intrusive at 2.3 km.

Belmont Porphyry Dikes

The Belmont Porphyry dikes contain abundant andesine feldspar with hornblende and lesser amounts of biotite in a dark-grey groundmass. The dikes strike to the northwest and are located throughout the district. The dikes were dated at 39.9$\pm$1.5 Ma using $^{40}K/^{40}Ar$ by Gulf Minerals Resources Co. in 1978.

Structural History

Major local structures in the MMD include normal faults, anticlines, synclines and grabens (Figure 6, Figure 7). Mapped structures are concentrated to the southwest of the Marysville stock. This could be due to poor outcropping in the MMD, but mining activity to the south-southwest of the Marysville stock has provided subsurface data in that area. The majority of local structures in the MMD

strike northwest-southeast, similar to the regional structures (Figure 6). The anticlines and synclines in the MMD formed temporally with the transpressional phase on the LCL (Figure 3) (Walker, 1992b). Normal faulting and graben development occurred temporally during transtension on the LCL and overprint the transpressional structures represented by earlier anticlines and synclines. The development of anticlinal doming is temporally synchronous with transtension. The doming of anticlines would be predicted with the change in regional stress fields because the rotation of principal stresses develops basin and dome structures (Ramsay & Huber, 1987). Walker (1992) proposed another hypothesis for the cause of anticlinal doming. Walker (1992) hypothesized that anticlines formed zones of structural weakness giving intrusives in the MMD a pathway through the crust and that the intrusion of igneous material caused doming of the anticlines. In both cases the doming of the anticlines in the MMD occurs during transtension.

Walker (1992) noted pre-mineralization, syn-mineralization, and post-mineralization stages of faulting in the MMD (Figure 8). The pre-mineralization faults strike to the northwest-southeast with moderate to vertical dips. This stage developed concurrently with anticlinal folds. The faults are primarily found along the axis of anticlines in the country rocks. The later Belmont Porphyry dikes follow these pre-mineralization structures. The syn-mineralization stage of faulting has two patterns: a dominant district scale pattern and subordinate local patterns. The dominant district scale pattern is an approximately radial pattern of normal faults that strike northeast to east, with the northeast striking faults in the north and east

striking faults in the south. The subordinate local patterns strike northwest and southeast and have moderate to steep dips. The post-mineralization stage of faults strike northwest-southeast with steep to vertical dips. These faults are generally dip slip and control graben development and other small, down-dropped blocks in the MMD.

Intrusive Events

The MMD records several intrusive events during Cretaceous and Eocene time. The Marysville stock, the largest known intrusive in the MMD, has a radiometric age date of 78 $\pm$ 4 Ma using $^{40}K/^{40}Ar$ (Baagsgaard et al., 1961a). Originally, the Marysville stock was thought to be the source of the gold mineralization in the MMD (Barrell, 1907). Gold mineralization was later proven to have occurred during the Eocene through cross-cutting relationships (Knopf, 1950a) and radiometric age-dating techniques (Walker, 1992b). There are three known intrusives with Eocene age dates in the MMD. The oldest Eocene intrusive is the Silver City Stock, radiometrically age-dated at 43.2 $\pm$ 2.6 Ma using $^{40}K/^{40}Ar$ by Petefish (1975). The Bald Butte pluton was radiometrically age-dated at 38.6 $\pm$ 1.5 Ma using $^{40}K/^{40}Ar$ by Gulf Minerals in the 1980s and is related to the molybdenum mineralization at the Bald Butte deposit. The Empire intrusive, located to the north of Bald Butte, also has molybdenite associated with it (Petefish, 1975) and a 40 Ma age date (Walker, 1992a). The Eocene intrusives are epizonal and appear to have been localized in the hinges of anticlines (Walker, 1992b). The tremolite and diopside metamorphic zoning around the Bald Butte and Empire Creek intrusions

(Figure 9) also supports an epizonal depth of emplacement. Petefish (1975) gave an emplacement depth of 2.3 km using fluid inclusion work for the Bald Butte and Empire intrusives. The previous work in MMD shows a bimodal distribution of intrusive events at ~80 Ma and 43-37 Ma with mineralization during the latter intrusive pulse.

Gold Veins

Walker (1992) (Figure 6) observed three preferred gold vein orientations in the MMD striking: (1) northwest-southeast, (2) northeast-southwest, and (3) east-northeast-west-southwest. The three gold vein sets have a systematic, spatial distribution around the Marysville stock. The northwest-southeast striking veins are located on the western side and the northeast-southwest striking veins are located on the southeast edge of the Marysville stock. Both of the veins sets are concordant with the contact of the Marysville stock. East-northeast-west-southwest striking veins are located along the anticline to the west of the Marysville stock (Figure 6). This vein set is perpendicular to the axial trace of the anticline. The three preferred gold vein orientations in the MMD appear to follow predicted orientations of structural weakness.

Historical Metal Production

Historic metal production data were compiled for the Bald Butte, Bell Boy, Big Ox, Drumlummon, Empire, Mammoth, and Strawberry, Penobscot, and Shannon mines in the MMD (Table 1). The data were used to show silver to gold ratios in the

different mines and the zoning of base metals in the MMD. The Bald Butte and Mammoth/Strawberry mines are the only two mines that produced more gold than silver (Table 1). The remaining mines in the MMD produced more silver than gold, but the ratio of silver-to-gold varied from ~21:1 to ~2:1 (Table 1). Based metals were also present in all of the mines except the Shannon. The historic ore grade at the Drumlummon mine was 0.5 oz. per ton with high-grade ore up to several ounces per ton (Walker, 1992a). Historically, roughly 1.1 million tons of ore have been produced from the Drumlummon mine (Walker, 1992a).

Recent Production at Drumlummon Mine

Recent assays on diamond drill core by RX Exploration at the Drumlummon mine indicate silver-to-gold ratios of ~13:1 to ~35:1 (Table 2) in mineralized quartz veins. Some of the new assay results have silver-to-gold ratios higher than the historical ratios for the Drumlummon mine. The higher silver-to-gold ratios in the new drill core may be because high-grade gold veins were the orignal target of historic production at the Drumlummon mine. Thus, early miners left behind veins with high silver-to-gold ratios. RX Exploration also conducted assays for As, Cu, Pb, Sb, and Zn on the diamond drill core for the newly discovered Charly vein. The assays show each of the base metals reaching up to 1 percent in the vein. As and Sb can reach concentrations up to 0.3 percent suggesting that the base metals (Cu, Pb, and Zn) are the main metals while As and Sb are the minor metals in the Charly vein. The total sulfide in the ore veins is low; generally less than 1 percent. The recent work by RX Exploration reflects the historic precious and base metal production in

the Drumlummon mine, while also providing insights into the minor metals occurring in the deposit.

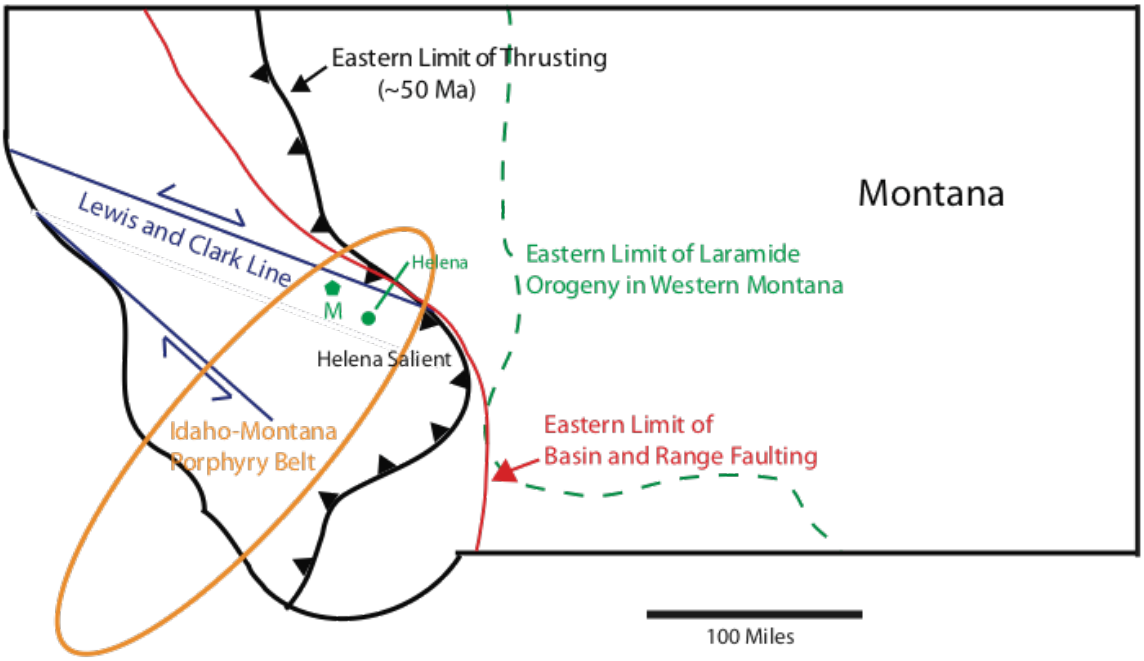

Figure 1: Generalized Geologic map of Montana showing the eastern limits of thrusting and Basin and Range faulting, the Lewis and Clark line and the location of the Marysville mining district, M–Marysville mining district. Armstrong et al., 1978, Rostad, 1978, Wallace, Lidke, and Schmidt, 1990, DeCelles, 2004, Lageson and Stickney, 2000.

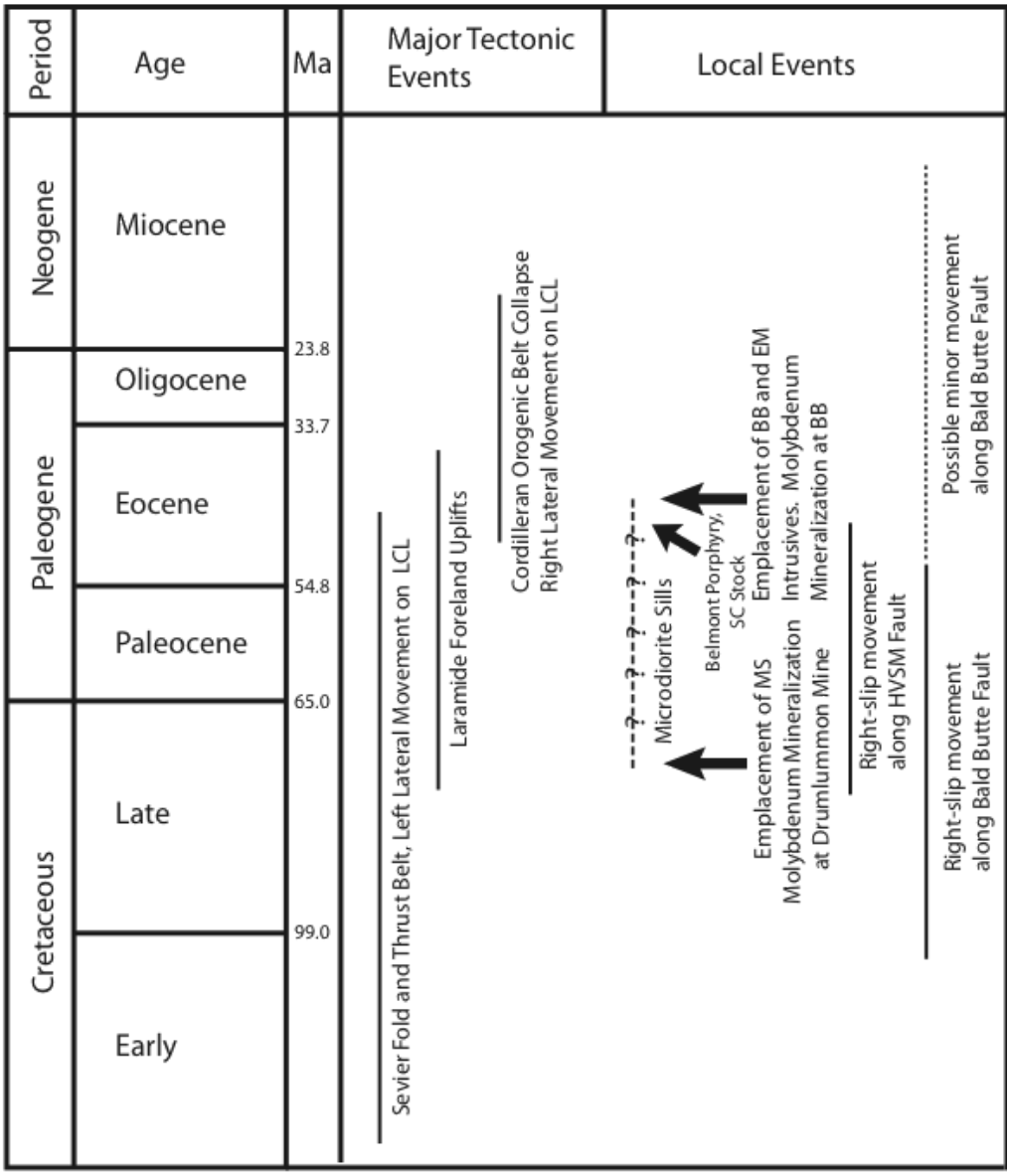

Figure 2: Timing of activity on regional structures and local events in the Marysville mining district from Cretaceous to Neogene time. MS-Marysville Stock, SC-Silver City Stock, BB-Bald Butte Intrusive, EM-Empire Mine Intrusive, HVSM-Helena Valley-Saint Mary. Data from: Dickinson, 2004, DeCelles, 2004, O'Neill et al., 2004, Hodges and Applegate, 1993, House, Bowring, and Hodges, 2002, McCay, 1978, Lageson and Stickney, 2000, Wallace, Lidke, and Schmidt, 1990, Walker, 1992.

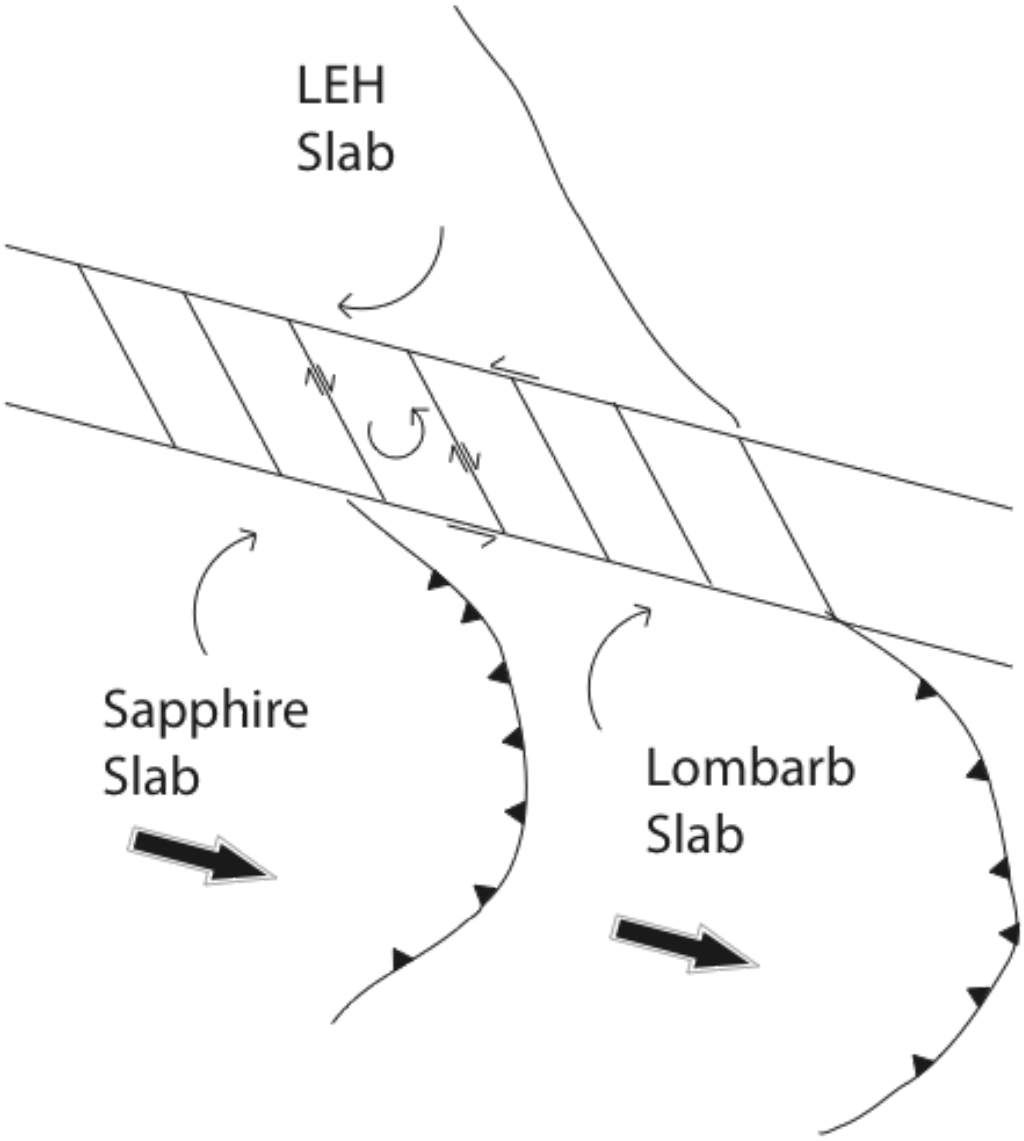

Figure 3: Simple shear model showing transpression on the LCL (Sears & Hendrix, 2004).

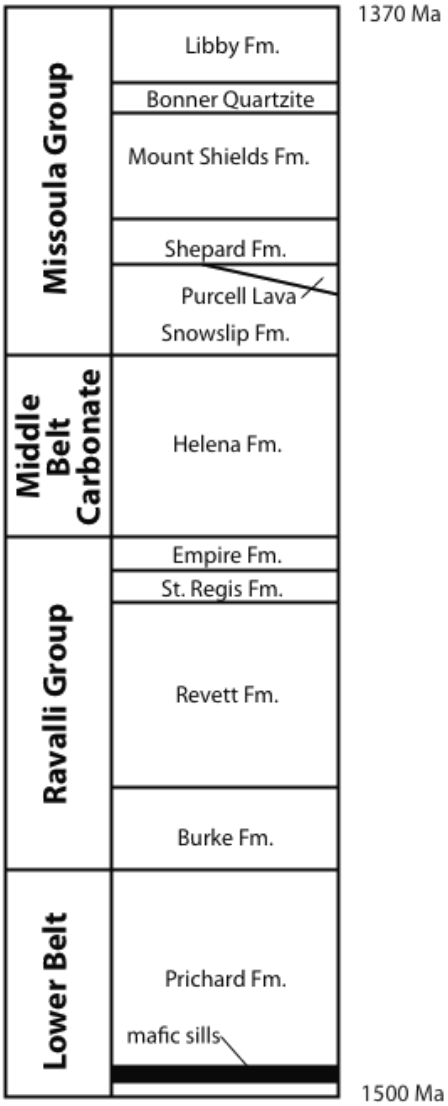

Figure 4: Belt Supergroup Stratigraphic column (Harrison et al., 1992).

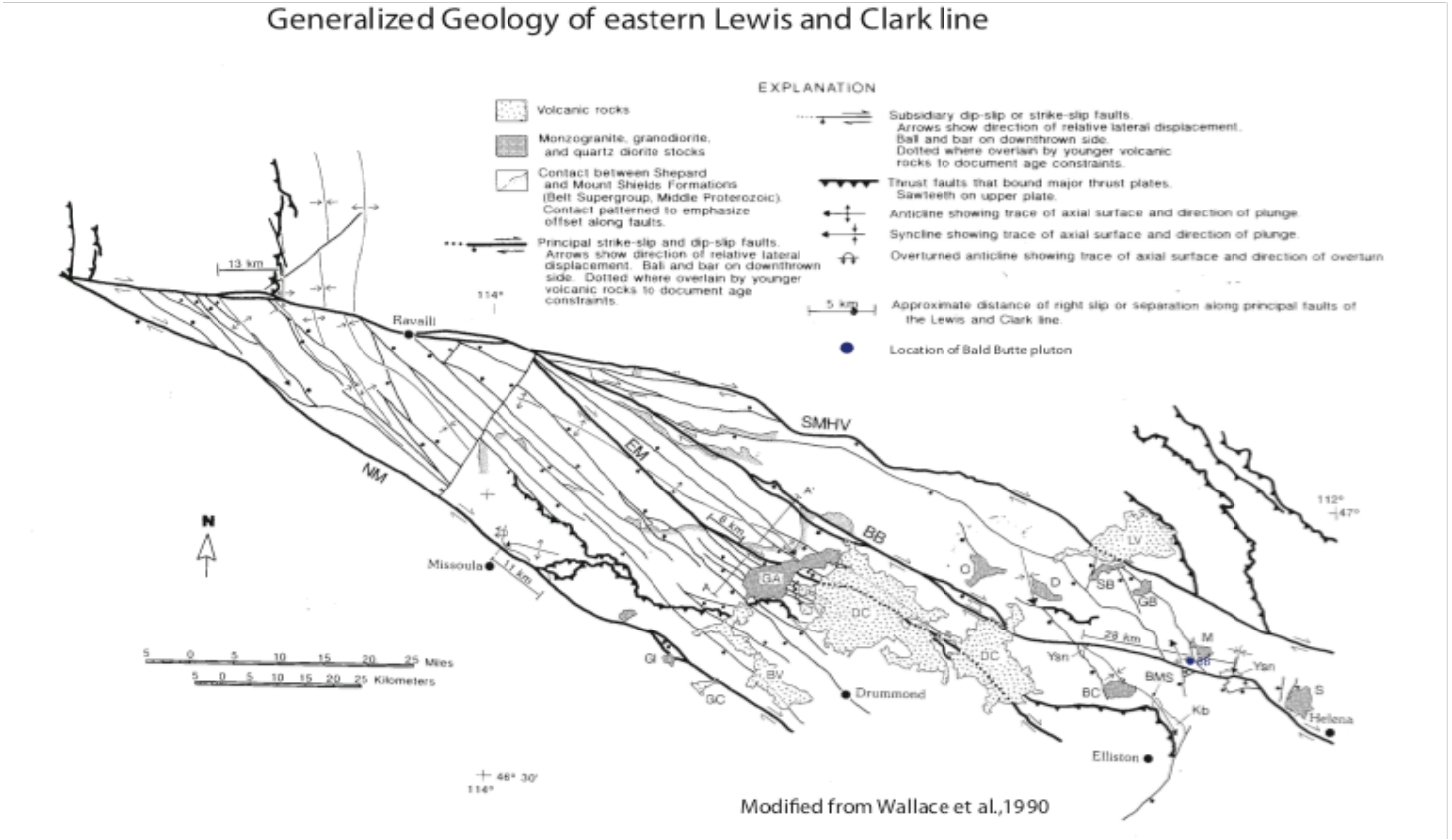

Figure 5: Map of the generalized structural relations in the central part of the Lewis and Clark line between the St. Marys-Helena Valley fault and the Ninemile fault. SMHV-St. Marys-Helena Valley fault; BB-Bald Butte fault; EM-Elevation Mountain fault; NM-Ninemile fault; BV-Bearmouth volcanic field (44-47 Ma); DC-Douglas Creek volcanic field (44-47 Ma); LV-Lincoln volcanic field (56 Ma); GC-Gillespie Creek volcanic field (50 Ma); GA-Garent stock (82 Ma); O-Ogden Mountain stock (81 and 85 Ma); D-Dalton Mountain stock (79 Ma); GB-Granite Butte stock (79 and 109 Ma); M-Marysville stock (78 Ma); BC-Blackfoot City stock (77 and79 Ma); S-Scratchgravel Hills stock (97 Ma); SB-Silver Bell stock (52 Ma); GI-Gillespie Creek stock (50 Ma). Kh-lower part of Blackleaf Formation folded in Black Mountain syncline (BMS). Ysn-Snowslip Formation in Black Mountain syncline, and in large fold north of the Bald Butte fault may indicate distance of separation. Modified from Wallace et al., 1990.

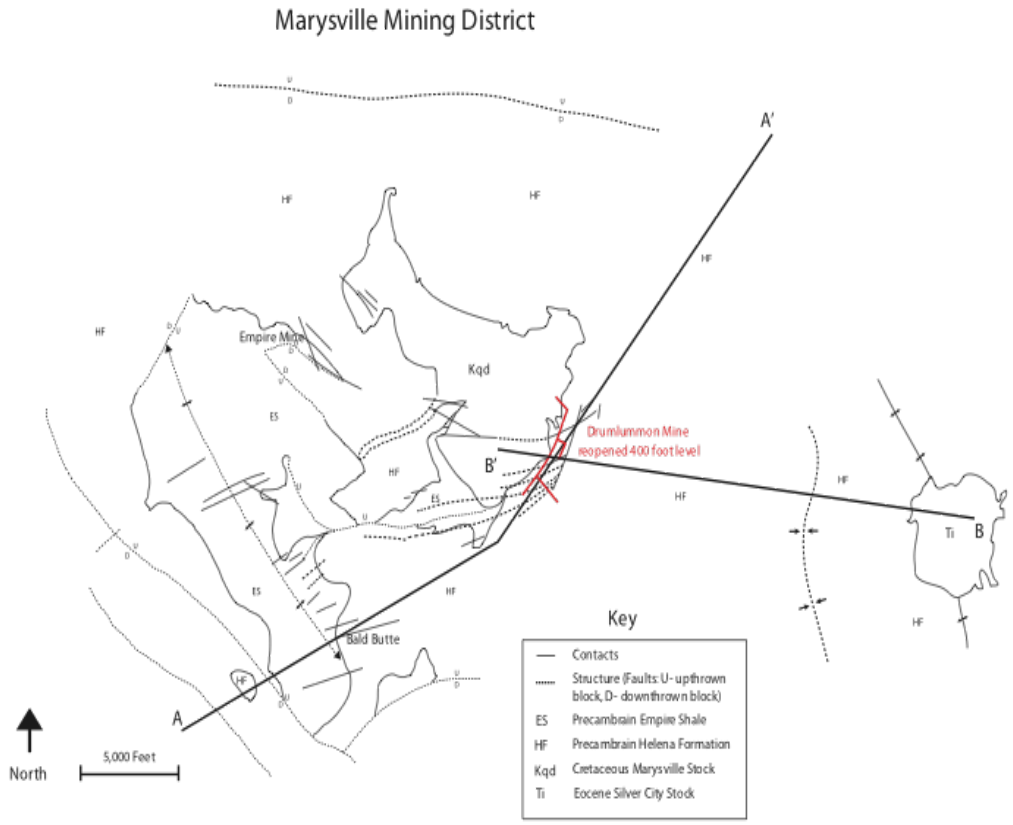

Figure 6: Map showing general geology of the Marysville Mining District. Country rocks consist of the Precambrian Belt Supergroup. Two intrusive events are found in the district, one during the Cretaceous and the other during the Eocene. Major structures in the district tend to follow a NW-SE pattern. Modified from Walker, 1992.

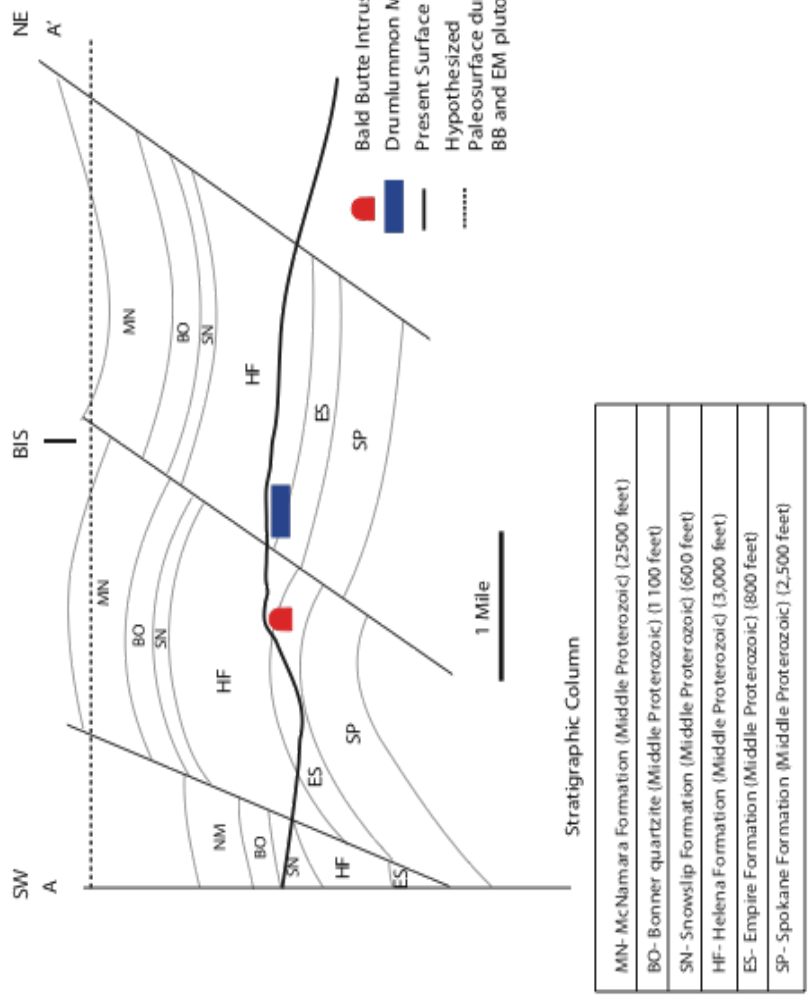

Figure 7: SW-NE Cross-section of the MMD showing the Bald Butte intrusion and Drumlummon mine. Paleosurface based on Petefish (1975). Major structures in the MMD are NW-SE normal faults.

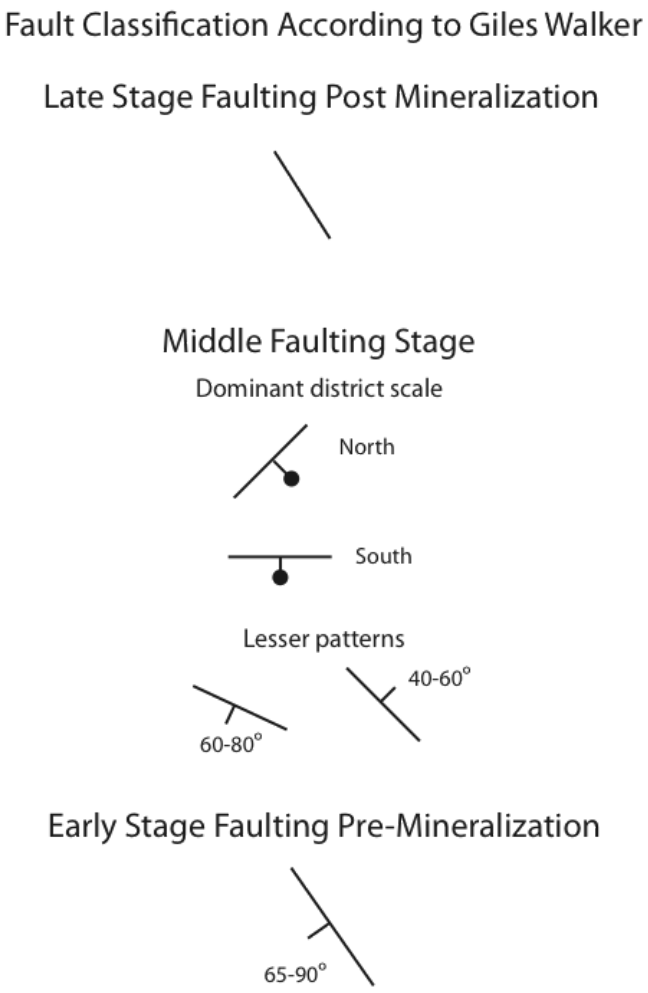

Figure 8: Faulting history in the MMD according to Walker (1992). Late stage faulting with steep to vertical dips and generally dip slip. Late stage faulting may control the Empire Creek graben and several other small, down-dropped blocks. Late stage faults offset veins of the Empire mine, Mount Pleasant, and Blue-Hickery-Shannon areas. Middle stage faulting has a somewhat radial pattern in the MMD and dips steep to vertical to the south. Middle stage faulting tends to be most prevalent on the SW contact of the Marysville stock. Strike lengths on middle stage faults are 12,000 to 15,000 feet. Displacements on faults are commonly normal and primarily dip slip. Early stage faulting developed concurrently with folding in the MMD, primarily occuring along the axis of the anticlines, or in between metasediments and the Marysville stock.

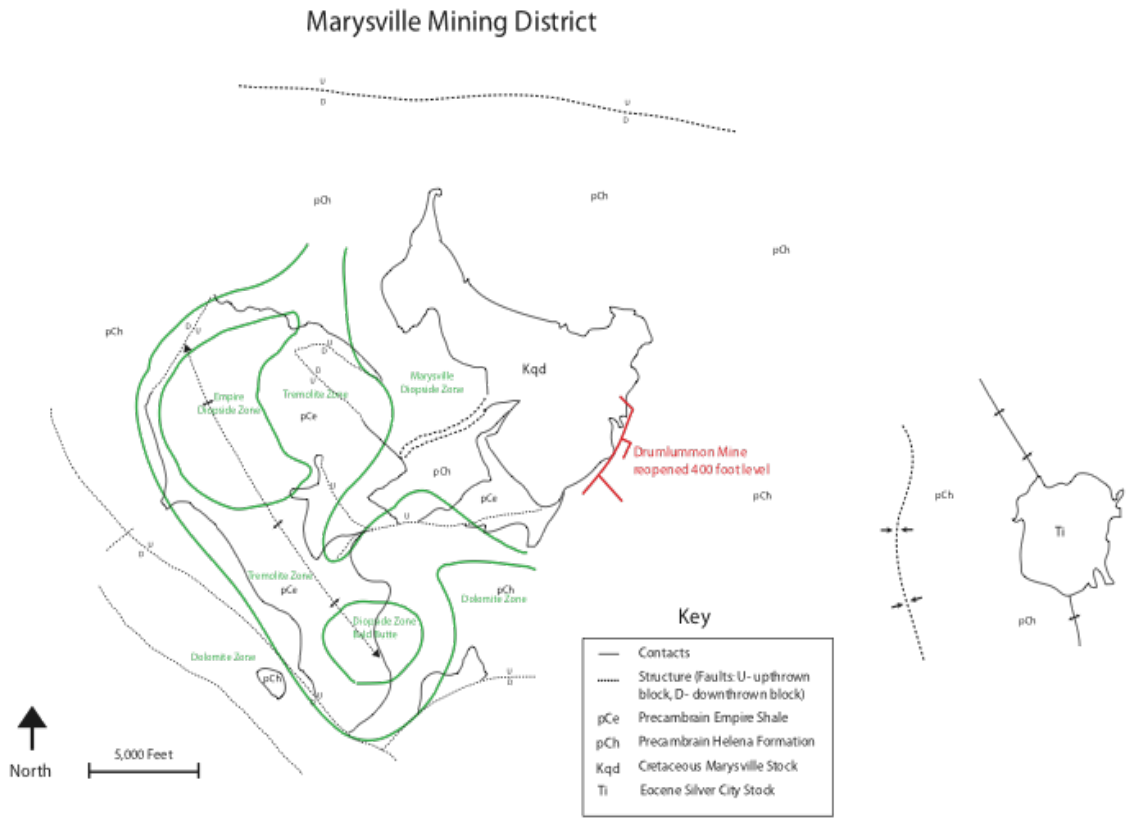

Figure 9: Map showing general geology of the Marysville Mining District. Country rocks consist of the Precambrian Belt Supergroup. Two intrusive episodes have been noted in the district; one during the Cretaceous and the other during the Eocene. Major Structures in the district follow a NW-SE pattern. Green lines show extent of diopside and tremolite alteration in the MMD. - Modified from Walker, 1992 and Petefish ,1975.

Table 1: Historical metal production in the MMD listed by mine Compiled from Walker (1992) and http://deq.mt.gov/abandonedmines/linkdocs/100tech.mcpx.

Mine Name	Gold (Oz)	Silver (Oz)	Silver/Gold Ratio	Copper (lb)	Lead (lb)	Zinc (lb)
Bald Butte	55390	49020	0.88	34814	290509	
Bell Boy	500	5154	10.30	35477	607224	21192
Big Ox	603	12794	21.21	6577	166982	24446
Drumlummon	115694	852666	7.37	23341	29848	
Empire	5683	19666	3.46	85839	1248168	36462
Mammoth+Strawberry	1960	519	0.26	193	161	
Penobscot	22560	57165	2.53	2072	18677	542
Shannon	31282	71847	2.29			

Table 2: Gold and Silver grades and ratios from recent drilling at the Drumlummon mine. From http://www.us-silver.com/Operations/Drumlummon/default.aspx.

Block	Estimated Tonnage	Grade Au (oz/ton)	Ounces of Gold	Grade Ag (oz/ton)	Ounces of Silver	Silver to Gold Ratio
A	67,284	0.39	26,192	12.2	820,166	31.3
B	39,740	0.53	21,097	7.3	291,053	13.8
C	48,494	0.48	23,414	16.6	804,341	34.6
Total	155,518		70,703		1,915,560	

GOLD DEPOSIT MODELS

Five major gold deposit types with corresponding models have been recognized in the North and South American Cordillera (Sillitoe, 2008): (1) epithermal, (2) porphyry, (3) sediment-hosted, (4) orogenic, and (5) pluton-related (Figure 10). A variety of tectonomagmatic controls are responsible for generating these different types of gold deposit. The tectonomagmatic controls are mineralizing intrusive-type, host rocks, depth of emplacement, temperature, and source of fluids (Table 3). It is typically not possible to directly infer the five tectonomagmatic controls listed above to differentiate among the deposit types. Instead, alteration minerals, gangue minerals, sulfide abundance and species, major and minor metals, and ore textures are used as a proxy (Table 4) (Sillitoe, 2008, Hedenquist, Arribas, & Ganzalez-Urien, 2000, Sillitoe & Hedenquist, 2003).

Epithermal

Epithermal gold deposits form in shallow volcanic environments, usually at depths between <500-1500 meters with temperatures ranging from 100-300^{O}C (Hedenquist et al., 1996). Typically epithermal deposits occur in volcanic rocks but they can be found in a wide variety of host rocks. The heat source and magmatic fluids in epithermal systems come from felsic igneous intrusions. Magmatic or heated meteoric fluids are accepted to be the mineralizing fluids forming epithermal deposits (Sillitoe, 2008, Hedenquist et al., 1996).

Epithermal gold deposits have been divided into three different subtypes:

high-sulfidation, intermediate-sulfidation, and low-sulfidation (Sillitoe & Hedenquist, 2003). The three subtypes of epithermal gold deposits have similar tectonomagmatic constraints. However, they differ by (1) alteration minerals, (2) gangue minerals, (3) sulfide abundance and species, (4) major and minor metals, and (5) ore textures (Hedenquist et al., 2000, Sillitoe & Hedenquist, 2003) (Table 4, Figure 11).

Mineralization in high-sulfidation epithermal deposits is produced by dominantly magmatic fluids (Sillitoe & Hedenquist, 2003) (Figure 12). The highly acidic magmatic fluids cause advanced argillic alteration (kaolinite + quartz + hematite + limonite) in the surrounding wall rocks. Key proximal minerals include quartz-alunite/aluminum phyllosilicates (APS) and, at depth, quartz-pyrophyllite/dickite. Gangue minerals are massive, fine-grained silica, vuggy residual quartz, and commonly late barite. Ore can be found in the form of stockworks, disseminations, veins, and/or breccias. Major metals are Au-Ag, Cu, and As. Minor metals include Zn, Pb, Mo, Sn, Hg, Bi, and W. The sulfide abundance will typically range from 10-90 percent and consists of enargite, luzonite, famatinite, and covellite.

Mineralization in intermediate-sulfidation epithermal deposits is thought to be derived from a mix of magmatic and meteoric fluids (Sillitoe & Hedenquist, 2003) (Table 3). Intermediate-sulfidation deposits have intermediate argillic $\pm$ adularia alteration with sericite as a key proximal mineral. The main gangue minerals consist of vein-filling crustiform quartz, comb quartz, and carbonates. Barite and

manganiferous silicates can be present locally as gangue minerals. Ore is found in the form of veins and stockworks. Major metals are Ag-Au, Zn, Pb, and Cu. Minor metals are Mo, As, and Sb. Sulfide abundance typically ranges from 5-20 percent and consists of sphalerite, galena, tetrahedrite-tennantite, and chalcopyrite.

Current research shows mineralization in low-sulfidation epithermal deposits to be derived from a mix of magmatic and meteoric fluids (Sillitoe & Hedenquist, 2003) (Table 3). Low-sulfidation deposits have intermediate argillic ± adularia alteration, with key proximal minerals being illite/smectite-adularia and roscoelite-illite-adularia. Gangue minerals are vein-filling crustiform quartz, colloform chalcedony, colloform quartz, and carbonates. Barite, celestite, and fluorite can also be locally present gangue minerals. Ore is in the form of veins and stockworks. Main metals in low-sulfidation systems are Au ± Ag. Minor metals are Zn, Pb, Cu, Mo, As, Sb, and Hg. Sulfide abundance is generally 1-10 percent in low-sulfidation deposits, but upwards of 20 percent sulfide can be seen if the deposit is hosted in basalt. The common sulfides species are galena, tetrahedrite-tennantite, and chalcopyrite; lesser sulfide species include arsenopyrite ± pyrrhotite and sphalerite.

Porphyry

Porphyry gold deposits form in a subvolcanic environment, usually at depths of 1-4 km (Singer, Berger, & Moring, 2008) and temperatures ranging from 300-600^{0}C. The deposits are hosted in a wide range of igneous rocks and country rocks.

However, they are typically hosted in quartz diorite to granodiorite porphyry stocks (Sillitoe, 2008). The mineralizing intrusives in porphyry gold deposits belong exclusively to I-type, magnetite series suites (Sillitoe, 2000). The mineralizing intrusives also provide the dominant mineralizing magmatic fluid source in porphyry gold deposits.

Porphyry gold deposits have the classic potassic, argillic, propylitic, and phyllic alteration pattern associated with porphyry systems (Lowell & Guilbert, 1970). Quartz is the dominant gangue mineral. Ore is always in the form of quartz stockworks with subordinate disseminated mineralization (Sillitoe, 1991). Major metals in porphyry gold deposits are Au and Cu; minor metals may be Mo and Ag. Sulfide abundance varies in the different alteration zones with 5-20 percent sulfide in the sericitic and propylitic zones, and 10-20 percent sulfide in advanced argillic zones (Sillitoe, 2000). The sulfides are dominantly pyrite and chalcopyrite, with a few deposits having bornite (Sillitoe, 1991).

Sediment-hosted (Carlin Type)

Sediment-hosted (Carlin Type) gold deposits are located in non-metamorphosed, carbonate-rich sedimentary sequences. Ore forming fluids are heated meteoric, metamorphic, and diluted magmatic fluids ranging in temperatures from ~180-240^{0}C. Deposits are emplaced at depths ranging from a minimum of ~1.7 to 6.5 km to a maximum of 5 to 8 km (Cline et al., 2005). Deep

crustal melting leading to prograde metamorphism and devolatilization produces the intrusions necessary to make sediment-hosted deposits.

Alteration processes in the host rocks are decalcification and silicification. Gangue minerals are pyrite, jasperiod, calcite, and quartz (drusy, chalcedony, amorphous). In some cases pyrite and jasperiod contain gold and are ore minerals. Ore is predominantly disseminated in style and controlled by a combination of faults and receptive stratigraphy. The major metals in sediment-hosted deposits are Au and Ag. Minor metals are As, Sd, Hg, and Ti. Sulfides consists of marcasite and pyrite, both of which can be ore minerals. Sulfide abundance is less than 3 percent in ore (Radtke, Rye, & Dickson, 1980).

Orogenic

Orogenic gold deposits are deposited at depths ranging from 3 to 15 km (Goldfarb, Groves, & Gardoll, 2001). The deposits are located in metamorphic rocks commonly assignable to greenschist facies. Mineralizing fluids are widely considered to lack a close genetic association with intrusions (Goldfarb et al., 2001). However, deeply sourced metamorphic and magmatic fluids remain viable sources of mineralizing fluids. During the formation of the ore deposit, temperatures reach 250-400^{O}C (Goldfarb et al., 2005).

The key alteration minerals in orogenic gold deposits include sericite and carbonate. The major gangue mineral is quartz. Ore in orogenic gold deposits is in the form of quartz veins and vein arrays. The major metals in orogenic gold deposits

are Au and Ag. Minor metals are As and Te. Ore contains 2-5 percent sulfide with the dominant sulfides consist of arsenopyrite and pyrite. Pyrrhotite can also be a main sulfide species in higher-temperature ores.

Pluton-related

Pluton-related gold deposits form deeper than epithermal deposits, but are still in the epizonal intrusive environment. Host rocks are felsic plutons and wall rocks surrounding the plutons. Pluton-related deposits are emplaced at depths of <1 to 6 km (Thompson et al., 1999). The temperature of ore formation is between 300-500^{0}C. Deposits are accepted to be the product of dominantly magmatic fluids.

Alteration minerals vary from alkali feldspar to sericite. The main gangue mineral is quartz with lesser amounts of K feldspar and/or albite. Ore form varies greatly and can be in the form of sheeted veins, stockworks, breccias, greisen-style alteration zones, pegmatite-aplite zones, skarn, replacements, veins, and shear zones. However, ore textures are most commonly simple structures characteristic of open space filling, ribbons, crack-seal textures, and breccias. Sulfide abundance is generally less than 5 percent and consists of pyrite, arsenopyrite, and pyrrhotite. Base-metal sulfides may also be present, but they are typically rare. In some deposits, base metals and sulfides (up to 10 percent) are found. The major metals in pluton-related deposits are Au$\pm$Ag. Minor metals are Bi, As, W, Mo, Te, and Sb.

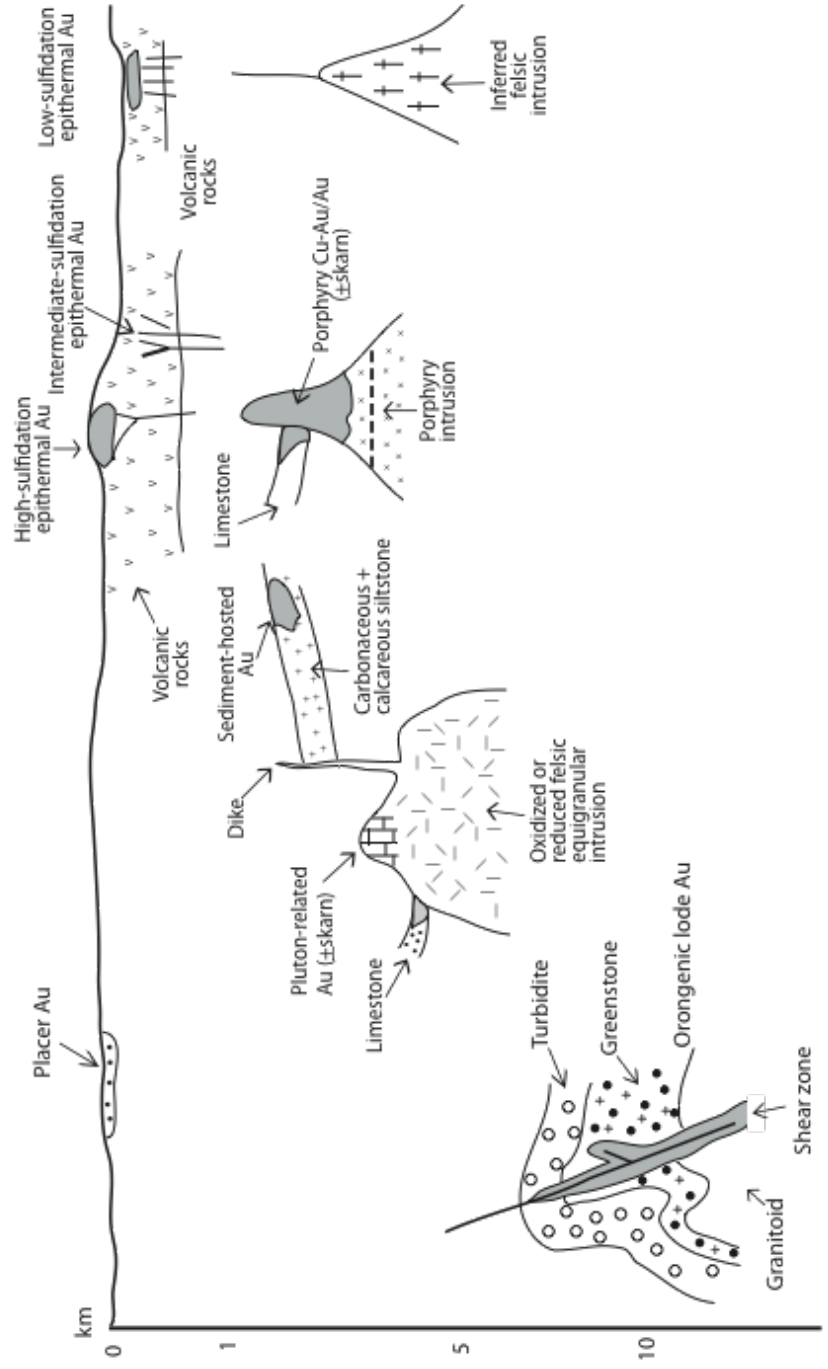

Figure 10: Gold deposit models for the Cordillera from Sillitoe (2008).

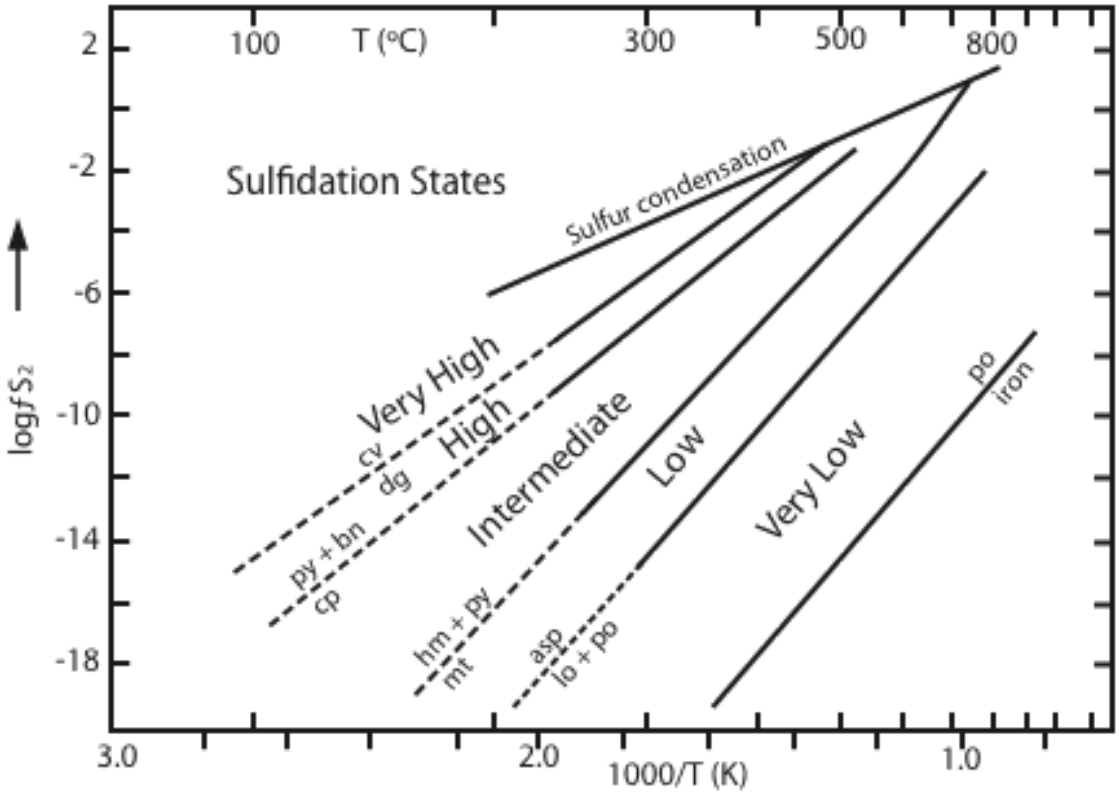

Figure 11: Log fS_2- 1,000/T diagram from Einaudi et al. (2003) defining the relative sulfidation states of hydrothermal fluids based on sulfidation reactions involving two or more copper- and iron-bearing mineral phases. cv-covellite, dg-digenite, py–pyrite, bn–bornite, cp–chalcopyrite, hm–specular hematite, mt–magnetite, asp arsenopyrite, lo–loellingite, po–pyrrhotite.

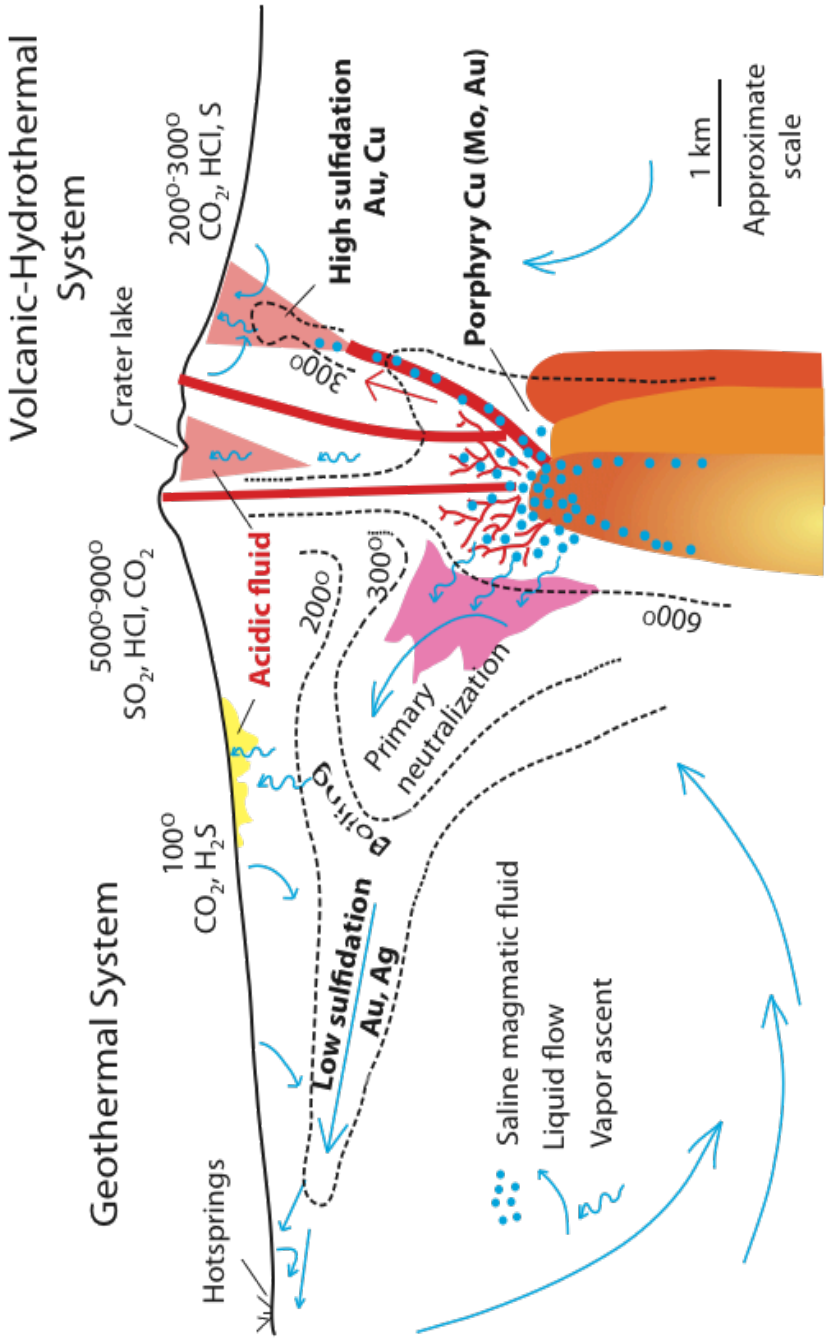

Figure 12: Deposit model showing low and high sulfidation Au systems. From Hedenquist et al. (1996).

Table 3: Tectonomagmatic controls on gold deposit from Sillitoe, 1998.

Gold deposit type	Principal mineralization style(s)	Characteristic accompanying elements	Typical host rocks	Typical proximal alteration type(s)	Ore fluid	Reference
High-sulfidation epithermal Au	Stockwork, disseminated, veins, breccias	Cu, As, Ag	Andesite to dacite volcanic rocks + basement	Advanced argillic	Mixed magmatic-meteoric	Simmons et al. (2005)
Intermediate-sulfidation epithermal Au	Veins, stockwork	Ag, Zn, Pb, Cu, As, Sb, Mn	Andestic to dacitic volcanic rocks	Intermediate argillic ± adularia	Mixed magmatic-meteoric	Simmons et al. (2005)
Low-sulfidation epithermal Au	Veins, disseminated	As, Sb, Zn, Pb	Felsic and basaltic volcanic rocks	Intermediate argillic ± adularia	Mixed magmatic-meteoric	Simmons et al. (2005)
Alkalic low-sulfidation epithermal Au	Disseminated, veins	Te, V, F	Alkaline volcanic rocks	Intermediate argillic ± adularia	Magmatic	Simmons et al. (2005)
Porphyry Cu-Au	Stockwork + disseminated	Mo	Quartz diorite to granodiorite porphyry stocks + wall rocks	Potassic, intermediate argillic, sericitic	Magmatic	Simmons et al. (2005)
Porphyry Au	Stockwork	Cu, Mo	Diorite to quartz diorite stocks + wall rocks	Potassic, intermediate argillic	Magmatic	Sillitoe (2000)
Skarn Au	Irregular to strata-bound replacements	As, Bi, Te, or Cu, Zn, Pb	Carbonate rocks	Calc-silicate	Magmatic	Meinert et al. (2005)
Reduced pluton-related Au	Sheeted veins, stockworks	As, Bi, Te, W, Mo	Felsic plutons + wall rocks	Alkali feldspar, sericitic	Magmatic	Thompson et al. (1999)
Oxidized pluton-related Au	Sheeted veins, stockworks	Zn, Pb, Cu, Mo	Felsic plutons + wall rocks	Alkali feldspar, sericitic	Magmatic	Sillitoe (1991)
Sediment-hosted Au	Dissminated	As, Sb, Hg, Ti	Impure carbonate rocks	Decalcification, silicification	Mixed magmatic-meteoric, meteoric, or metamorphic	Cline et al. (2005)
Orogenic Au	Veins, stockworks	As, Te	Greenschist-facies metavolcano-sedimentary rocks	Sericite (Cr mica)-carbonate	Metamorphic and/or deep-seated magmatic	Goldfarb et al. (2005)

Table 4: Characteristics of gold deposits.

Gold deposit type	Typical proximal alteration type(s)	Gangue mineral(s)	Sulfide abundence and species	Main metals	Minor metals	Ore textures	Reference
High-sulfidation epithermal Au	Advanced argillic	Massive fine-grained silicification, vuggy residual quartz, late barite common	10-90% sulfide, enargite, luzonite, famatinite and covellite	Au-Ag, Cu, As	Zn, Pb, Bi, W, Mo, Sn, Bi	Stockworks, disseminations, veins and/or breccias	Sillitoe and Hedenquist (2003)
Intermediate-sulfidation epithermal Au	Intermediate argillic ± adularia	Quartz, carbonate Local: barite, manganiferious silicates	5-20% sulfide, sphalerite, galena, tertahedrite-tennantite, chalcopyrite	Ag-Au, Zn, Pb, Cu	Mo, As, Sb	Veins and stockworks	Sillitoe and Hedenquist (2003)
Low-sulfidation epithermal Au	Intermediate argillic ± adularia	Quartz, carbonate Local: barite, celectie, flourite	1-10% sulfide, Main: galena, chalcopyrite tertahedrite-tennatite Minor: sphalerite, arsenopyrite ± pyrrhotite	Au±Ag	Zn,Pb, Cu,Mo, As,Sb, Hg	Crustiform and colloform quartz, colloform chalcedony	Sillitoe and Hedenquist (2003)
Porphyry Cu-Au	Potassic, intermediate argillic, sericitic	Quartz	5-20% sulfide, pyrite, chalcopyrite, bornite	Au, Cu	Mo, Ag	Stockworks, minor dissemination	Sillitoe (2000), Sillitoe (1991)
Pluton-related Au	Alkali feldspar, sericitic	Quartz Minor: K feldspar, albite	<5% sulfide, pyrite, arsenopyrite, pyrrhotite	Au±Ag	Bi, As, W, Mo, Te, Sb	Open space filling textures, ribbons, crack-seal textures	Thompson et al. (1999), Thompson and Newberry (2000)
Sediment-hosted Au	Decalcification, silicification	Pyrite, calcite, quartz, jasperiod	<3% sulfide, Pyrite, marcasite	Au, Ag	As, Sd, Hg, Ti	Disseminations	Cline et al. (2005), Radtke et al. (1980)
Orogenic Au	Sericite (Cr mica)-carbonate	Quartz	2-5% sulfide, Arsenopyrite, pyrite, pyrrohotite	Au, Ag	As, Te	Quartz veins, vein arrays	Goldfarb et al. (2005)

CONTROLS ON EPITHERMAL ORE BODIES AND VEIN GEOMETRIES

Two criteria have been developed to explain the controls on ore emplacement in epithermal deposits: first, based on ore body geometry (Sillitoe, 1993), second, based on ore grade (Hedenquist et al., 2000). Data from the Drumlummon mine was evaluated for both criteria to determine if ore emplacement was structurally, hydrothermally, or lithologically controlled.

Ore Body Geometry

The Sillitoe (1993) criterion states that the low pressure and hydrostatic conditions in which epithermal deposits are formed produce extremely variable ore body geometries—meaning that ore body geometries in epithermal deposits are typically controlled by permeability differences in the host rocks. Different ore body geometries can be linked to the three permeability inducing processes. The permeability inducing processes are controlled by either lithology, structure, or hydrothermal processes (Sillitoe, 1993) (Figure 13).

Structural Controls

Four ore body geometries have been identified to be the result of structural control: (1) massive vein, (2) vein swarm, (3) stockwork, and (4) low-angle veins (Figure 13). Massive veins up to tens of meters wide form when a fault is active for extended periods of time coinciding with the influx of mineralizing fluids. Vein

swarms form in a similar environment to massive veins. However, a vein swarm forms when the vein becomes stronger than the wall rock or the fault splays. This results in the new faults forming and becoming filled with mineralizing fluids over an extended period of time. Stockworks tend to develop in brittle lithologies that have experienced strike-slip faulting due to the shattered faulting and fracture patterns that develop in this structural setting. Bulk-tonnage stockworks may also develop in hanging walls of steep normal faults. Low-angle veins can form under two separate processes: ring faults and gravity-induced faults. Ring faults are developed around calderas or diatremes. Veins are formed following the favorable pathways at intersections of district-wide normal faults and the ring faults. Also, gravity-induced faults in a caldera environment can form veins where structures have shallow dips toward or away from the fluid source. Structural controls can occur pre- and concurrently with mineralization.

Hydrothermal Controls

Two different geometric types of ore bodies have been identified to be the result of hydrothermal control: (1) hydrothermal breccia and (2) residual vuggy silica (Figure 13). Hydrothermal brecciation can often be an important mechanism for the formation of ore deposits. As a result, extensive studies have been done on the subject (Jebrak, 1997). Generally, permeability caused by hydrothermal activity is the result of fluid overpressure during syn-mineralization faulting creating a hydrothermal breccia. Hydrothermal breccias may extend beyond these faults. Rock leaching can also occur as the highly acidic magmatic fluids move through the wall

rocks creating residual vuggy silica. This creates permeability in the form of vugs where the leached minerals were present and a residual vuggy silica texture is left.

Lithologic Controls

Lithologic controls on ore bodies occur when permeable strata are receptive to mineralizing fluids. Impermeable strata may also help focus mineralizing fluids in the permeable layers. The ore body shape will take the form of the permeable stratigraphic layers with ore disseminated in the layers (Figure 13). There are three different geologic settings that can lead to ore being lithologically controlled. The first occurs when mineralizing fluids are intruded into poorly lithified rocks that were deposited just prior to or during mineralization (Figure 13). An example of this would be a volcanic setting with ignimbrite deposits occurring just before or concurrently with emplacement of the mineralizing intrusive. The second type of lithologic control occurs where there are stratigraphic discontinuities. A common example of this is regional unconformities with less permeable strata below and more permeable strata above. In this setting mineralizing fluids accumulate above horizons of reduced permeability (Figure 13). The third way for ore body to be lithologically controlled is when ore is localized in a permeable diatreme breccia (Figure 13).

Ore Grade and Tonnage

The Hedenquist et al. (2000) criterion uses ore grade and tonnage to define the controls on epithermal gold deposits (Figure 14). The Y-axis on Figure 14 is the grade of the deposits and is a function related to the focusing process on the ore veins. The X-axis is the tonnage of the deposits, which is a function of the length of the hydrothermal activity and geology of the deposit. Epithermal gold deposits can be divided into three categories using the Y-axis of the chart: (1) low-grade, (2) medium-grade, and (3) high-grade. The use of both the Y-axis and the X-axis will determine if a deposit is economic or not. A key difference between high- and low-grade deposits is a change in deposit form from veins (high-grade) to disseminations (low-grade). Deposits in the form of veins have a strong focusing process while deposits in disseminated form lack this strong focusing process. This indicates that controls on high-grade deposits are structural, while low-grade deposits are dominantly lithologically controlled. The structural focusing process in high-grade epithermal deposits is typically in the form of fracture control (Hedenquist et al., 2000). Thus, a good understanding of the origin of the faults and fractures is important and may be critical during exploration for fault-controlled, high-grade deposits (Hedenquist et al., 2000).

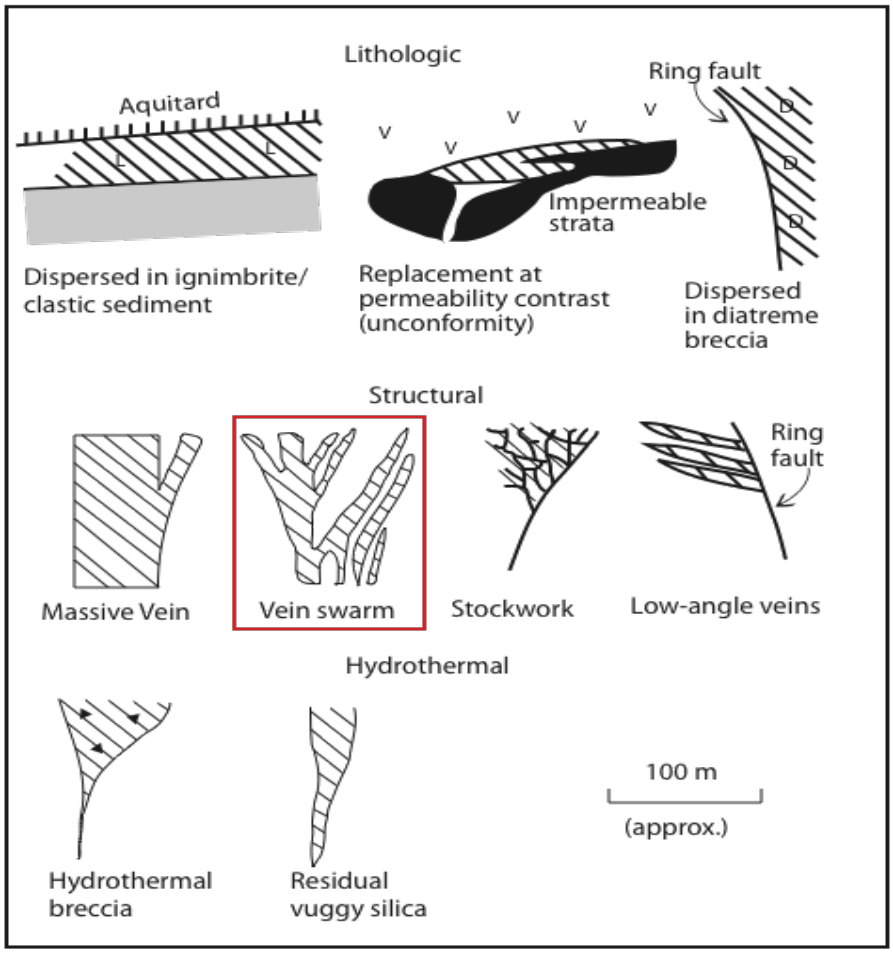

Figure 13: Common ore body forms showing three main controlling processes; lithologic, structural, and hydrothermal. Ore depicted by angled lines. Red square indicates best fit for the ore body shape at the Drumlummon mine. Modified from Sillitoe (1993).

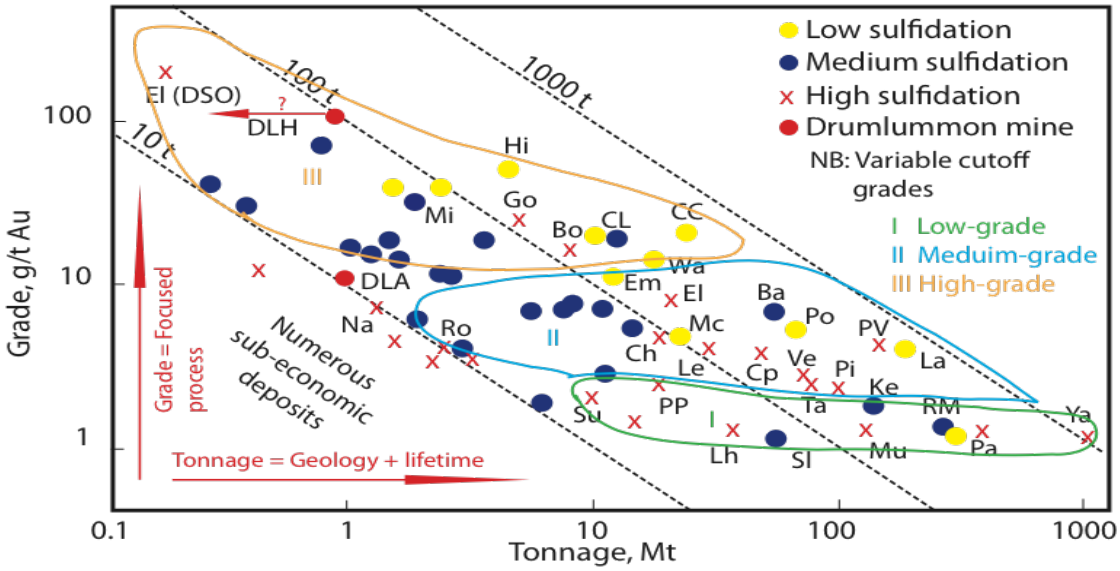

Figure 14: Grade-tonnage plot of low-sulfidation and high-sulfidation epithermal ore deposits (modified from Hedenquist et al., 2000). Includes both production and reserves but with various cut-off grades. Note that there are many prospects that contain low tonnages and/or grades, plotting in the lower left corner, which are largely uneconomic to mine. Drumlummon mine production data from Walker (1992). The red arrow from the DLH shows area where the high grade would plot since exact amount of production is not known. Intermediate sulfidation-state deposits such as Comstock Lode and Kelian are shown with the low-sulfidation symbol. I = Low-grade, disseminated, oxidized, or leachable ore; II = Medium-grade, unoxidized, and refractory deposits; III = Structurally controlled, high-grade veins or lodes; Ba = Baguio, Philippines; Bo = Boliden, Sweden; CC = Cripple Creek, Colorado; Ch = Chinkuashih, Taiwan; CL = Comstock Lode, Nevada; Cp = Chelopech, Bulgaria; DLA = Drumlummon (average-grade ore), Montana; DLH = Drumlummon (high-grade ore), Montana; El = El Indio, Chile; EL DSO = El Indio direct-shipping ore; Em = Emperon, Fiji; Go = Goldfield, Nevada; Hi = Hishikari, Japan; Ke = Kelian, Indonesia; La = Ladolam, Papua New Guinea; Lh = Lahoca, Hungary; Le = Lepanto, Philippines; Mc = McLaughlin, California; Mi = Midas, Nevada; Mu = Mulatos, Mexico; Na = Nansatsa district deposits, including Kasuga, Japan; Pa = Pascua, Chile; Pi = Pierina, Peru; Po = Porgera, Papua New Guinea; PP = Paradise Peak, Nevada; Sl = Sleeper, Nevada (average-grade ore); Su = Summitville, Colorado; Ta = Tamba, Chile; Ve = Veladero, Argentina; Wa = Waihi, Martha Hill, New Zealand; Ya = Yanacocha, Peru.

METHODS

Field Mapping

Structural measurements were taken for fractures, veins, dikes, striations, and faults during both outcrop and underground field mapping. Structures were projected to waist level during the underground mapping. Relative-age relationships of structures were also recorded. Measurements were gathered with a Brunton compass, ruler, and a 10x hand lens. Structural attitudes of planes were recorded using the right hand rule. The right hand rule states that the dip of a plane is 90 degrees clockwise from the reported strike. Thus, a set of near-parallel, steeply dipping veins could include veins with both northeast and southwest strikes. Striated surfaces were measured using a protractor to measure the rake of the striation on the striated surface. Since the majority of fractures and veins recorded were steeply dipping, they were plotted on rose diagrams instead of stereonets to provide a better visualization of the planes.

Field mapping was completed in three phases in the MMD. One phase was conducted on the district scale focusing on fracture patterns. Two smaller areas were mapped in greater detail: the 400-foot underground level of the Drumlummon mine and the altered area around the Bald Butte intrusive (Figure 6, end of Chapter One). Mapping around the Bald Butte intrusive was broken into two parts: (1) vein patterns around the pluton and (2) kinematic relationships of veins and faults in a small, open-pit, surface mine. The Drumlummon underground mapping focused on

structural relationships and lineation orientations on striated surfaces with the objective of completing a paleostress reconstruction. Data collection was not uniform in each area because of inconsistent quality of outcrops and underground exposures. Collected data were then used to compile a partial deformational history of the MMD.

Geochronology

Rhenium-Osmium Geochronology

Re-Os analyses were carried out at the Applied Isotope Research for Industry and the Environment (AIRIE) geochronology laboratory at Colorado State University -Fort Collins under the direction of Dr. Holly Stein. This section describes standard methods used in this lab (Stein, 2011, personal communication).

The Re-Os chronometer in molybdenite has been established as an accurate and precise age-dating method for molybdenite mineralization (Stein et al., 2001). The Re-Os chronometer method produces accurate and precise dates because molybdenite usually contains Re in the ppm range and essentially no initial Os when mineralization occurs. With time the Re will decay into Os with a known half life. Because of this we are able to take the ratio of Re to Os to determine the age of the sample. The Re-Os chronometer in molybdenite has also been shown to be robust through ductile deformation and thermal metamorphism up to granulite grade metamorphism (Bingen & Stein, 2003, Stein et al., 2004, Stein & Bingen, 2002). However, Re and Os can be decoupled in molybdenite (Stein et al., 2003) causing

inaccurate age dates if proper lab procedures are not followed. The decoupling problem is overcome by targeted drilling to capture complete grains of molybdenite and later fully homogenizing the individual grains.

Upon acquiring an acceptable molybdenite sample, a Carius tube digestion was used (Shirey & Walker, 1995). The molybdenite was dissolved and equilibrated with a mixed double Re-double Os spike (^{185}Re-^{188}Os-^{190}Os) in HNO3-HCL (inverse *aqua regia*) by heating it for 12 hours at 230^{0}C in a sealed, thick-walled glass ampoule (Markey et al., 2003). The double spike permits a dual check for common Os and a mass fractionation correction, leading to highly precise results. The Os is recovered by distilling directly from the Carius tube *aqua regia* into HBr and is subsequently purified by micro distillation. The Re is recovered by anion exchange. The Re and Os are located on the Pt filaments. Isotopic compositions are determined using NTIMS on NBS 12-inch radius, 68^{0} and 90^{0} sector mass spectrometers at Colorado State University. Two in-house molybdenite standards, calibrated at AIRIE, are run routinely as an internal check (Stein et al., 1997, Markey, Stein, & Morgan, 1998). Blanks are also routinely monitored at AIRIE and data are always reported as blank-corrected values. After the ppm of Re and Os were acquired from the sample, the age was calculated by applying the equation $^{187}Os=^{187}Re(e^{\lambda t} - 1)$, where λ is the decay constant for ^{187}Re and t is the calculated age. The ^{187}Re decay constant of 1.666×10^{-11} yr^{-1} was used with an uncertainty of 0.31 percent (Smoliar, Walker, & Morgan, 1996). Reported 2σ errors include the propagation of all uncertainties, including the uncertainty in the ^{187}Re decay constant.

$^{40}Ar/^{39}Ar$ Thermochronology

$^{40}Ar/^{39}Ar$ analyses were carried out at the New Mexico Geochronology Research Laboratory (NMGRL) at the New Mexico Bureau of Mines and Geology in Socorro under the direction of Dr. Matthew Heizler. The standard laboratory procedures and modeling methods used are described in Appendix A.

Ore Mineralogy FEM-EDS

An ore mineralogy study was completed using samples from the Drumlummon, Charly, Christmas, and Castleton gold-bearing veins in the Drumlummon mine. Samples for the ore mineralogy study were selected from drill core and made into polished thin sections by Vancouver Petrographics (Figure 15). The polished thin sections were then analyzed using an optical microscope to identify potential ore minerals. Once potential ore minerals were identified, a spot analysis was completed using a Zeiss Supra 55 VP Field-emission Electron Microscope (FEM) with a Noran Energy Dispersive X-ray Spectrometer (EDS) in the Image and Chemical Analysis Laboratory (ICAL) at Montana State University. Each spot analysis result was labeled in the following fashion: vein_#A, where vein = the ore vein that the sample was taken from (Ch = Christmas, DL= Drumlummon, Cr = Charly, Ca = Castleton); # = subsection on the thin section containing a group of analyzed minerals; and A = the individual spot analyzed. The EDS analysis gave both weight and atomic percents of the elements present in the spot analyzed. The silicon and oxygen in the analysis are assumed to be generated from the electron beam

penetrating the glass of the thin section slide because only opaque minerals were analyzed. Consequently Silicon and oxygen were removed from the results. Ratios of atomic percents for the remaining elements were used to identify the ore minerals present.

Paleostress Analysis

Currently there are two widely applied criteria used as the basis for paleostress reconstruction: the Wallace and Bott criterion of minimum misfit angles (Bott, 1959, Wallace, 1951) and the Mohr-Coulomb criterion (Mohr, 1900, Coulomb, 1776). Wallace (1951) and Bott (1959) showed that the direction of slip on any plane with a known orientation (n) can be predicted under a given stress tensor σ, assuming that the slip takes place parallel to the direction of the maximum resolved shear stress (s):

$$s = \sigma \cdot n - (n^T \cdot \sigma \cdot n)\, n$$

where superscript T is the transpose of the matrix. The Mohr-Coulomb Criterion states all faults are active when shear stress (τ) overcomes some critical value ($\mu\sigma_n$),

$$\tau = C + \mu\sigma_n$$

where C is the cohesion and μ is the coefficient of friction. The T-Tecto program (Zalohar & Vrabec, 2007) was used in this study since it allows for both paleostress reconstruction methods to be used. With both methods a minimum of nine faults

should be used to have statistical confidence in the paleostress reconstruction (Orife & Lisle, 2006).

One of the best-known and widely used graphical techniques to visualize paleostresses is the Right Dihedra method described by Angelier and Mechler (1977) (Figure 16). This method uses the Wallace and Bott criterion of minimum misfit angles to complete a paleostress reconstruction. The Right Dihedra Method is based on the assumption that faults active in the same stress field have a common intersection of the pressure (P) and tension (T) quadrants. It is also assumed that the orientation of the maximum principal stress axis (σ_1) is constrained to the P quadrant and the orientation of the minimum principal stress (σ_3) is constrained to the T quadrant. The spatial orientation and position of the P and T quadrants are defined by orientation of the fault plane and the slip direction along it. Overlapping the P-T quadrants for each fault plane solution, constrains the orientation of σ_1 and σ_3 as the geometrical center of the common intersection of the P and T quadrants (Figure 16). One limitation of the Right Dihedra Method is that it cannot produce actual magnitudes and directions of principal stress axes because the solution is not unique and does not include information regarding the relative size of the principal stresses (Angelier, 1979).

The Gauss method (Zalohar & Vrabec, 2007) uses a variation of the Mohr-Coulomb Criteriona and the Mohr-Navier shear failure criterion to complete a paleostress reconstruction. The Mohr-Navier shear failure criterion is advantageous

because results are in agreement with Amonton's Law (Angelier, 1989, Jaeger & Cook, 1969), which states:

$$\tau \geq \mu\sigma_n = \tan\phi_2 \cdot \sigma_n$$

where μ is the coefficient of residual friction for sliding on a preexisting fault, and σ_n is the normal stress on the fault. The basic theory behind Amonton's law is that a fault plane is activated only when shear stress exceeds some critical value $\mu\sigma_n$, which represents the frictional shear strength. In the Mohr diagram the points representing the values of normal and shear stress on the faults lie above the straight line $\tau = \mu\sigma_n = \tan\phi_2 \cdot \sigma_n$ (Figure 17). The stresses in the Earth's crust related to faulting are usually compressive. Thus, the area on the Mohr diagram where the points can lie is located below the straight line $\tau = \tan\phi_1 \cdot \sigma_n$ (Figure 17). This line represents the tangent of the largest Mohr circle on the Mohr diagram. The parameter ϕ_1 approximates the shear strength of an intact rock which can be approximated by the Coulomb-Navier shear failure criterion (Jaeger & Cook, 1969, Ranalli & Yin, 1990):

$$\tau = S + \sigma_n \cdot \tan\phi_i.$$

Here, S is the cohesive strength and ϕ_i is the angle of internal friction. The advantage of using the Coulomb-Navier shear failure criterion is that the results given have stress tensors. Thus, acceptable results from the Coulomb-Navier method can then be compared to the results from using the Right Dihedra Method as a means to crosscheck.

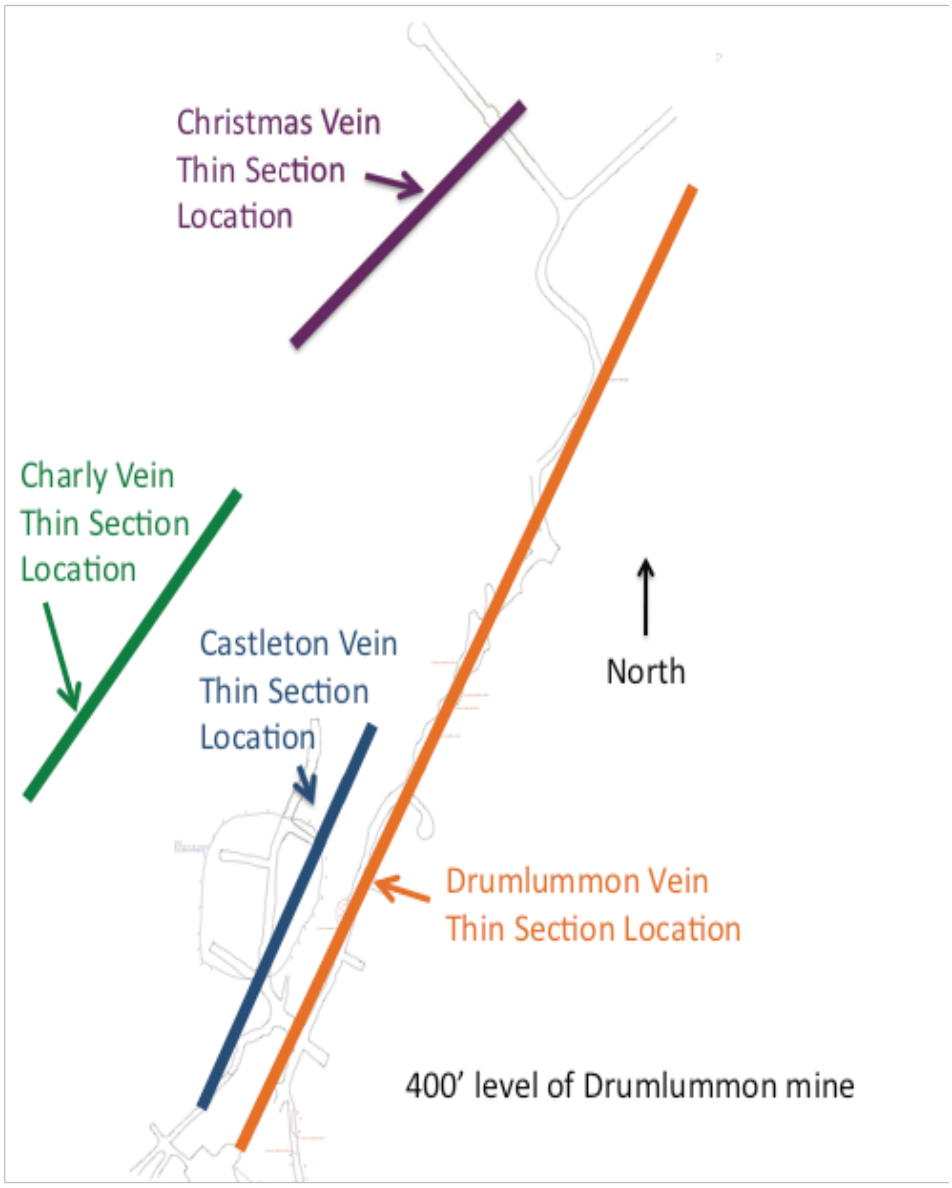

Figure 15: Thin section sample locations for ore mineralogy study on the 400 Level of the Drumlummon mine.

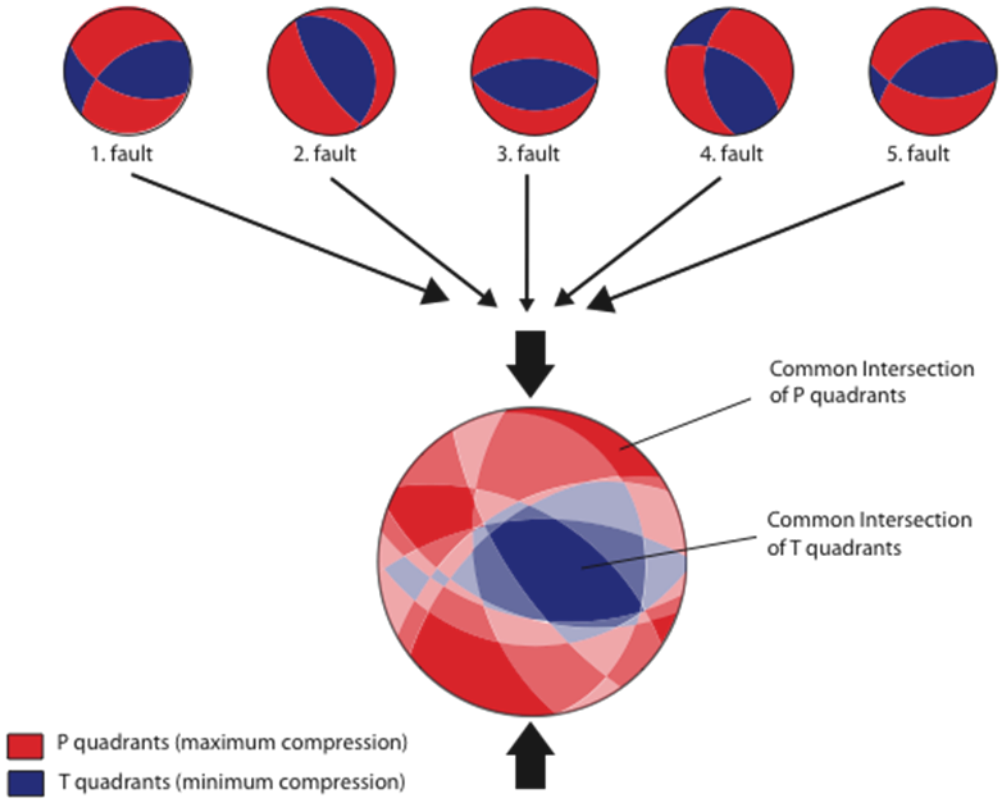

Figure 16: Visualization of the basic principal behind the Right Dihedra Method. From Angelier and Mechler, 1977.

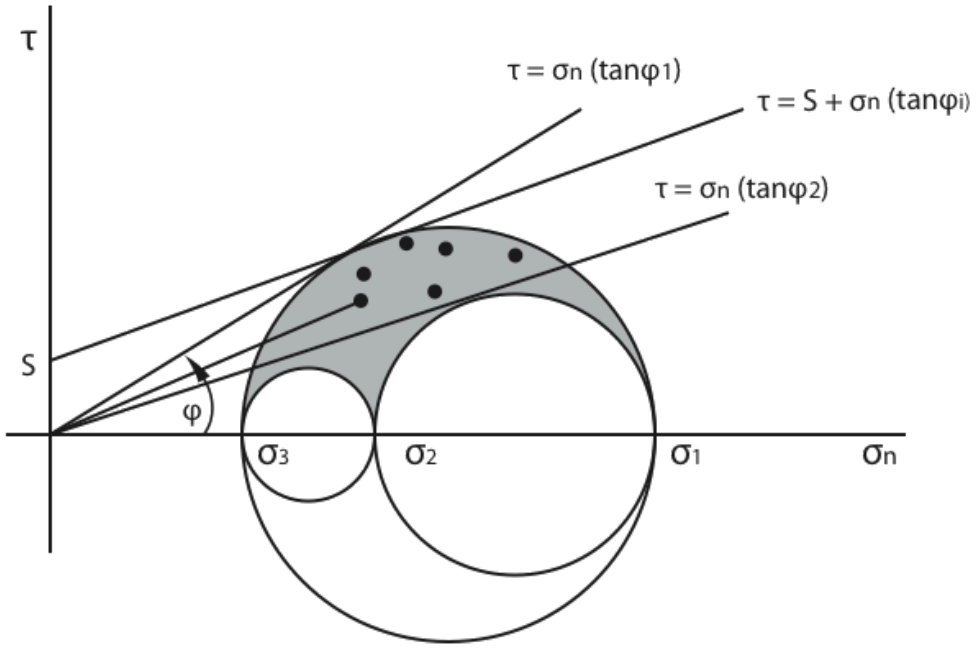

Figure 17: Mohr diagram illustrating normal (σ_n) and shear stress (τ) on the faults (black points). σ_1, σ_2 and σ_3 represent principal stress magnitudes and S is the cohesion. The position of the points for all possible fault orientations is restricted to the gray area. However, for mechanically acceptable solutions the position of the points is additionally restricted to the area between the two straight lines with equations $\tau = \sigma_n \cdot \tan \phi_2$. The first represents the tangent of the largest Mohr circle and roughly approximates the angle of internal friction ϕ_I for an intact rock, and the second represents the Amonton's law.

RESULTS

Structural Mapping: Veins, Dikes, Fractures, and Faults

Marysville District: Fracture and Vein Mapping

The district scale mapping focused on fractures, but also included veins, dikes, and faults. The fracture data was broken into domains in and around the Marysville stock (Figure 18) (Appendix C). The domains were established based on the uniformity of fracture orientation and their relation to larger scale features in the MMD. A total of six fracture domains were established in the MMD; five in the country rock and one in the Marysville stock. In each domain the fracture sets were further classified as major or minor based on frequency of the fractures. Both major and minor fracture sets were recorded in the Marysville stock. The major set is orientated northwest-southeast and the minor set is orientated northeast-southwest (Figure 18). The A and B domains are both located to the west of the Marysville stock and both contain an east-northeast-west-southwest set of major fractures. Also, the A domain has a north-northwest-south-southeast major fracture set and Domain B has south and west-northwest-east-southeast major fracture sets (Figure 18). The C, D, and E domains to the east of the Marysville stock all contain both northeast-southwest and northwest-southeast fracture sets. However, the northwest-southeast fracture set is only a major set in the D domain and it is the minor set in the C and E domains (Figure 18). The northeast-southwest fracture set

is a major set in all three domains. A north-south fracture set is also a major fracture set in the D and E domains.

Bald Butte Vein Mapping

Mapping at the small open-pit mine at Bald Butte revealed three vein sets cut by late stage faults (Appendix E). The first (oldest) vein set consists of northeast striking quartz±molybdenite veins dipping 80° to 90°. No movement indicators were observed in the first set of veins. The second vein set consists of roughly east-west striking veins dipping ~20°-40° that contain both quartz±molybdenite and quartz+clay veins. Both dextral and sinistral movement indicators were recorded on the second vein set. The third (youngest) vein set consists of northwest to north-northeast striking veins containing both quartz±molybdenite and quartz+clay veins dipping 70° to 85°. Dextral and sinistral movement was recorded on the third vein set as well. The youngest structures observed were late stage faults striking southeast and dipping 40° to 60°. Along the late stage faults, sense of displacement was difficult to determine but appeared to be normal.

Field mapping around Bald Butte focused on the orientation of veins and other small-scale structures in outcrop. Only a limited amount of data was provided from field mapping since natural outcrop exposures in the Bald Butte area is quite poor. Three orientations of mineralized and un-mineralized quartz veins were prevalent in the map area: (1) Steeply dipping, southwest-striking veins (2) Steeply dipping, southeast-striking veins (3) Steeply dipping, east-west-striking veins (Figure 19) (Appendix D). The absence of shallow dipping veins in natural outcrops

could be explained due to the fact that they are more likely to be exposed in the vertical walls of the open pit than in the low-relief natural exposures. The majority of veins mapped were quartz veins with no visible mineralization. However, molybdenite was observed in all three vein generations. Cross-cutting relationships in the field show that the southwest and the southeast vein sets bracket the east-west vein set in age. This is consistent with the veining relationship seen in the open pit mapping. Both sinistral movement and dextral movement were recorded in the southwest and southeast vein sets. The displacements across the veins are minor and show no signs of brittle deformation suggesting movement occurred during vein emplacement. A spatial variation in the orientation of veins is seen in relation to Bald Butte and the underlying Bald Butte intrusive (Appendix D). In the area to the southeast of Bald Butte the the east-west striking vein set is predominant. However, the southwest striking vein set predominates to the northeast of the intrusive. Overall the major orientation of veins around Bald Butte is southwest striking with steep dips (Figure 19).

Drumlummon Mine: Underground Mapping

Structures mapped underground in the 400-foot level of the Drumlummon mine include fractures, veins (mineralized and non-mineralized), dikes, minor faults, and lithologic contacts. During the underground mapping, special attention was paid to mapping relative ages of structures and striated surfaces. Once the mapping was finished a structural and intrusive history of the mine was put together based on cross-cutting relationships. Five distinguishable, intrusive and

structural episodes were identified (Figure 21, Plate A in Appendix F). From oldest to youngest the episodes are: (1) intrusion of felsic dikes, (2) mineralized and non-mineralized veins, (3) northeast- and southwest-striking normal faults and right lateral strike-slip faults, (4) east-west-striking normal faults, and (5) north-northeast-striking left lateral and west-striking right lateral strike-slip faults.

The felsic dikes strike to the southeast with average dips around 55°-60° and have been dated at 78.1±0.5 Ma (Appendix A) using $^{40}Ar/^{39}Ar$ on primary sericite. Mineralized and non-mineralized veins were intruded after emplacement of the felsic dikes. The veins mapped are small scale, generally less than 1 foot, and are not large enough to be mineable ore veins. There are two sets of veins striking to the northeast and southwest with mineralization seen in both sets. The northeast-striking, mineralized veins mapped are aligned parallel to the ore veins in the Drumlummon mine. The main gangue minerals in the mineralized veins are quartz and carbonate with lesser amounts of chlorite and clays. This is consistent with the gangue minerals in the ore veins at the mine. Structural movement was observed after the emplacement of the dikes and veins. Three stages (3-5) of minor faulting were recognized during the observed structural movement (Figure 21). The stage 3 faults have normal and strike-slip kinematics. The stage 3 normal faults are orientated northeast and southwest, and the strike-slip faults are orientated south to southwest and northeast with right lateral movement. Stage 4 faulting consists of a different episode of normal faults orientated east and west. The final stage (stage 5) of faulting consists of strike-slip faults that are orientated east-west with right

lateral movement and northeast with left lateral movement. Reverse faults were mapped in bends along the stage 5 strike-slip faults. New workings in the 450-level of the Drumlummon mine revealed that the Drumlummon structure also has a releasing bend consistent with left lateral movement on the structure.

Hornfels is present throughout the Drumlummon mine and is thought to be related to the intrusion of the Marysville stock (Rice, 1977). Skarn was mapped on the 400 level and a newly excavated decline to the 450 level in the Drumlummon mine. The skarn postdates the hornfelsing from the Marysville stock and small-scale vein emplacement. Lighter colored layers in the Helena formation (most likely reflecting the more carbonate rich layers in the formation) were most receptive to skarn formation. Major proximal alteration minerals related to gold mineralization include chlorite, clays, and adularia.

Ore veins were also studied during the underground mapping and from historic maps. Ore veins did not have residual vuggy silica. The veins are hosted in hornfels, with the exception of the Northstar vein that is located in the Marysville stock and post-dates the hornfelsing event. Veins cut across banding in the hornfels. Ore-bearing veins range in size from 2-10 meters wide and are spaced 8-85 meters apart. The ore veins generally strike to the northeast with the exception of the Northstar vein that strikes to the northwest. The dip on ore veins averages 60°-70° to the southeast.

Ore Mineralogy

An ore mineralogy study was completed using samples from the Drumlummon, Charly, Christmas, and Castleton gold-bearing veins in the Drumlummon mine (Table 6) (Appendix B).

Christmas Vein

Analysis of the Christmas vein revealed no precious-metal-bearing minerals. Only base metal minerals were identified. The base metal minerals are galena and sphalerite (Table 6). The Ch_1a-c, Ch_2d, Ch_4a-b, and Ch_5a spot analyses showed lead and molybdenum in the samples. However, the Kα peak, inner shell transition x-ray wavelengths for the two elements were close together, meaning the signal for molybdenum could have been interpreted from the lead peak shoulder. To differentiate between lead and molybdenum, the outer shell x-ray wavelengths (L and M peaks) for these elements were examined. There is a lack of either the L or M peak for molybdenum, suggesting that no molybdenum is present and the entire Kα peak represents lead. Thus, molybdenum was removed from the data and the molybdenum counts were assigned to the lead peak. Also, the Kα peaks for lead and sulfur are close together possibly causing sulfur peaks to be incorrectly counted as lead peaks. These samples were checked using reflective light microscopy to confirm whether they are indeed native lead or galena. The samples identified by FEM-EDS as native lead showed classic triangular polishing pits using reflective light microscopy. These are indicative of galena. Thus, the spot analyses were

interpreted as being galena. The Ch_2b, Ch_2c, and Ch_5b spot analyses had a sulfur to zinc ratio of ~2:3. This ratio does not match the pure sphalerite sulfur to zinc ratio of 1:1. However, volatilization of sulfur is common under an electron beam and leads to lower counts of sulfur in comparison to the actual amount present. The slightly lower ratio of sulfur to zinc would be expected for a sphalerite sample with the possibility of sulfur volatilization. Thus, results from the spot analyses were interpreted to indicate that the mineral is sphalerite.

Castleton Vein

The analysis of the Castleton vein found five precious-metal-bearing minerals in the sample: (1) acanthite-argentite, (2) chalcopyrite with silver, (3) jalpaite, (4) stromeyerite, and (5) freibergite (Table 6). The spot analysis of Ca_1a had a sulfur-to-silver ratio of ~1:4, and a minor amount of magnesium was also present. This ratio doesn't match the pure acanthite-argentite sulfur-to-silver ratio of 1:2, but it is still interpreted as acanthite-argentite with sulfur volatilization leading to lower counts of sulfur. The spot analyses of Ca_1c, Ca_2a and Ca_6b had sulfur-to-iron ratios of ~2:1, sulfur-to-copper ratios of ~2:1, and sulfur-to-silver ratios ranging from 2:1-40:1. The analyzed sulfur-to-iron matches the pure chalcopyrite sulfur-to-iron ratio of 2:1. The analyzed sulfur-to-copper ratio matches the pure chalcopyrite sulfur-to-copper ratio of 2:1. Having silver as a trace element in the chalcopyrite is consistent with previous studies (Fleischer, 1955). The spot analyses of Ca_1b and Ca_1d had a sulfur-to-silver ratio of ~2:3 and a sulfur-to-copper ratio of ~2:1. The analyzed ratios of Ca_1b and Ca_1d are consistent with jalpaite. The spot analysis of

Ca_4c had a sulfur-to-copper-to-silver ratio of ~1:1:1. This is consistent with stromeyerite that has a sulfur-to-copper-to-silver ratio of 1:1:1. The spot analysis of Ca_5c had a sulfur-to-copper-to-silver ratio of ~2:1:2. The analyzed ratio does not match any known mineral. However, the sample could be stromeyerite that is depleted in copper. The Ca_6a spot analysis had a sulfur-to-copper ratio of ~1:1 and a sulfur-to-antimony ratio of ~1:4. Minor amounts of silver and zinc were also present in the sample. The sulfur-to-copper ratio is consistent with the pure form of freibergite sulfur-to-copper ratio of 1:1. The sulfur-to-antimony ratio is a bit lower than the pure form ratio of 1:3. However, the sample ratio of sulfur to antimony is within an acceptable range to be considered freibergite.

Analysis of the Castleton vein also revealed four base-metal minerals: (1) chalcopyrite, (2) galena, (3) sphalerite, and (4) tetrahedrite (Table 6). The Ca_2b, Ca_2c-d, Ca_3b, and Ca_5a-b spot analyses had ratios for sulfur to copper to iron ranging from ~2:1:1 to ~5:3:3. The analyzed minerals were interpreted to be chalcopyrite with a slightly lower amount of sulfur than the pure form ratio of sulfur to copper to iron of 2:1:1. The Ca_1e spot analysis had a sulfur-to-copper-to-iron ratio of ~4:1:1. This analysis is also thought to be of chalcopyrite with a higher amount of sulfur. The Ca_3a, Ca_3c-d, and Ca_4b spot analyses only contained lead. However, the Kα peaks for lead and sulfur are also close together causing sulfur to be counted as lead. Samples were checked using reflective light microscopy to confirm or deny whether they were native lead. When samples identified as native lead by FEM-EDS were checked with reflective light microscopy they showed classic

triangular polishing pits indicative of galena. Thus, the Ca_3a, Ca_3c-d, and Ca_4b spot analyses were interpreted to be galena. The Ca_4a and Ca_4d spot analyses had a sulfur-to-zinc ratio of ~2:3 and the Ca_5e spot analysis gave a sulfur-to-zinc ratio of ~2:1. The analyzed ratios for Ca_4a, Ca_4d, and Ca_5e were interpreted to be sphalerite with slightly higher or lower sulfur-to-zinc ratios than the pure sphalerite sulfur-to-zinc ratio of 1:1. The Ca_6c spot analysis had a sulfur-to-copper ratio of ~2:3 and a sulfur-to-antimony ratio of ~1:6. The analysis was interpreted to be tetrahedrite with a sulfur-to-copper ratio a bit higher than the pure tetrahedrite ratio of 1:1. Also, the sulfur-to-antimony ratio is slightly higher than the pure tetrahedrite ratio of 1:3.

Drumlummon Vein

The analysis of the Drumlummon vein revealed five precious-metal-bearing minerals: (1) chalcopyrite with silver, (2) stromeyerite, (3) silver copper sulfide, (4) argentite-acanthite, and (5) native copper with minor sulfur and silver (Table 6). Carbonate alteration was noted during optical microscopy on the Drumlummon thin section. Backscattered electrons from the carbonate alteration minerals would be expected to show up in the analysis if the spot analysis was close to carbonate alteration. Elements from alteration (Ca, Mg) were removed whenever the spot analyzed was close to the carbonate alteration. The spot analyses of DL_1a, DL_2e-f, and DL_4c had a ratio of sulfur to iron to copper of ~2:1:1 and sulfur-to-silver ratios ranging between 7:1 and 200:1. The analyzed sulfur-to-iron-to-copper ratios of ~2:1:1 were consistent with the pure chalcopyrite sulfur to-iron-to-copper ratio of

2:1:1. Minor silver in the chalcopyrite is consistent with previous studies that have trace amounts of silver associated with chalcopyrite (Fleischer, 1955). The spot analysis of DL_2b had a sulfur-to-silver-to-copper ratio of ~1:1:1. These ratios are consistent with stromeyerite. The spot analysis of DL_3a had a sulfur-to-silver-to-copper ratio of ~1:2:2. The spot analysis of DL_3f gave a sulfur-to-silver-to-copper ratio of ~2:2:1. The two samples had a lower amount of copper and sulfur than pure stromeyerite, but are still within an acceptable range to be interpreted as stromeyerite. The DL_2d spot analysis had a sulfur-to-silver ratio of ~1:7 and a copper-to-silver ratio of ~1:7. This mineral is interpreted to be native silver with minor amounts of copper and sulfur. The spot analyses of DL_2g and DL_3b gave a sulfur-to-silver ratio of ~1:2 to ~3:4. Minor amounts of aluminum and copper were also present. The range of ratios is consistent with the pure argentite-acanthite ratio of 1:2. The DL_2a, DL_2h, DL_3c, and DL_3g spot analyses had sulfur-to-copper ratios ranging from ~1:20 to ~1:60 and silver-to-copper ratios ranging from ~1:20 to ~1:40. These analyses are interpreted to be native copper with minor amounts of silver and sulfur.

The analysis of the Drumlummon vein also had three base-metal minerals: (1) chalcopyrite, (2) galena, and (3) sphalerite (Table 6). The DL_4a-b, DL_5b-c, and DL_6a spot analyses had sulfur-to-copper ratios ranging from ~1:1 to ~3:4 and sulfur-to-iron ratios ranging from ~3:5 to ~3:4. The analyzed ratios are consistent with chalcopyrite pure form having sulfur-to-iron and sulfur-to-copper ratios of 1:2. The DL_1d spot analysis had a lead-to-zinc ratio of 14:1 and a lead-to-aluminum

ratio of 1:10. However, the Kα peaks for lead and sulfur are close together and can cause sulfur to be counted as lead. The sample was checked using reflective light microscopy to confirm or deny whether this spot was indeed native lead. When the DL-1d spot analysis was checked with reflective light microscopy, it showed classic triangular polishing pits indicative of galena. Thus, the spot analyses have been interpreted to be galena with minor amounts of zinc and aluminum. The DL_1c and DL_e1 spot analyses gave a sulfur-to-zinc ratio of ~2:3. Minor amounts of aluminum were also detected in the samples. The analyzed spots are interpreted to be sphalerite with a slightly higher amount of zinc than the pure sphalerite ratio of 1:1 for sulfur to zinc.

Charly Vein

The analysis of the Charly vein had eight precious-metal-bearing minerals: (1) chalcopyrite with silver, (2) sphalerite with silver, (3) pyrite with silver, (4) argyropyrite, (5) stromeyerite, (6) acanthite-argentite, (7) silver zinc sulfide, and (8) geffroyite (Table 6). The spot analyses of Cr_ 3b and Cr_7a had sulfur-to-iron-to-copper ratios ranging from ~2:1:1 to ~3:2:2. Minor amounts of silver were also present. The analyzed ratios are consistent with the pure chalcopyrite sulfur-to-iron-to-copper ratio of 2:1:1. The minor silver in the chalcopyrite is consistent with previous studies that have silver associated with chalcopyrite (Fleischer, 1955). The Cr_7b spot analysis had a sulfur-to-zinc ratio of ~1:1; minor amounts of iron and silver were also present. The analyzed ~1:1 sulfur-to-zinc ratio is consistent with the pure sphalerite sulfur-to-zinc ratio of 1:1. The Cr_1c, Cr_2c, Cr_2f, Cr_1d, Cr_1e,

Cr_1h, Cr_2a, and Cr_7c spot analyses had sulfur-to-iron ratios ranging from ~2:1 to 3:2 with minor amounts of silver present. The analyzed sulfur-to-iron ratios are consistent with the pure pyrite sulfur-to-iron ratio of 2:1. The spot analysis of Cr_la had a sulfur-to-iron ratio of ~3:1 and a sulfur-to-silver ratio of ~9:1 with minor amounts of calcium and magnesium present. The analyzed sulfur-to-iron ratio of 3:1 has slightly more sulfur than the pure argyropyrite sulfur-to-iron ratio of 11:7. The analyzed sulfur-to-silver ratio of 9:1 has more sulfur than the pure argyropyrite sulfur-to-silver ratio of 11:3. The analyzed ratios for Cr_1a are still within an acceptable range to be interpreted as argyropyrite. The spot analyses of Cr_1i, Cr_2b, Cr_3d, Cr_6a, and Cr_6d had sulfur-to-iron-to-silver ratios of ~1:1:1. The analyzed sulfur to-iron-to-silver ratio is consistent with the pure stromeyerite sulfur-to-iron-to-copper ratio of 1:1:1. The spot analyses of Cr_2d, Cr_3c, and Cr_3d had sulfur-to-silver ratios ranging from ~1:2 to ~5:7 with minor amounts of iron also present. The analyzed ratios for sulfur to silver are consistent with the pure acanthite-argentite sulfur-to-silver ratio of 1:2. The spot analysis of Cr_5b had a sulfur-to-zinc-to-silver ratio of ~3:1:3. No known mineral has this composition. The spot analyses of Cr_5d, Cr_6c, and Cr_7d had sulfur-to-silver ratios of ~1:1 to ~3:4. The analyzed ratios for sulfur to silver are consistent with the pure form of geffroyite.

Analysis of the Charly vein had sphalerite as the only base-metal mineral (Table 6). The spot analyses of Cr_5a and Cr_7e had sulfur-to-zinc ratios of roughly ~2:3 and ~1:2 with minor amounts of iron or calcium also present. The analyzed

ratios have slightly higher sulfur-to-zinc ratios than the pure sphalerite ratio of 1:1 for sulfur to zinc.

Isotope Geochronology

Two different isotope age-dating techniques were used in this study, ^{187}Re-^{187}Os and $^{40}Ar/^{39}Ar$, to date mineralization and constrain relative age dates compiled during mapping.

Rhenium-Osmium Geochronology

Two samples were selected to age-date using the Re-Os chronometer in molybdenite. The samples were collected from the Drumlummon mine and the Bald Butte molybdenum prospect (Figure 6, at end of Chapter One). The molybdenite sample collected in the Drumlummon mine was in a quartz vein located on the margin of the newly discovered Charly gold vein. The cross-cutting relationship between the Charly vein and molybdenite-bearing vein cut by the Charly vein gives evidence for the molybdenite-bearing quartz vein being emplaced before the Charly vein. The molybdenite sample from the Drumlummon mine gives an age of 79.6 $\pm$ 0.6 Ma (Table 2, at end of Chapter One). The Bald Butte molybdenite sample was collected from a stockwork quartz vein in the potassically altered zone of the deposit. The Bald Butte molybdenite sample gives an age of 39.9 $\pm$ 0.1 Ma (Table 2).

$^{40}Ar/^{39}Ar$ Thermochronology

Two samples were collected from the Drumlummon mine for $^{40}Ar/^{39}Ar$ thermochronology. The two samples collected were adularia from the Charly vein

and muscovite from a felsic dike. The felsic dike contained primary muscovite, biotite and potassium feldspar. The biotite was altered; however, the muscovite and potassium feldspar were unaltered and interpreted to be primary. Both the muscovite and potassium feldspar were selected with the idea that the potassium feldspar would be used if ages given by the muscovite were in question. The adularia sample from the Charly vein was contaminated with calcite and did not yield a useful result. The muscovite felsic dike sample yielded an age date of 78.1±0.5 Ma.

Paleostress Analysis

A paleostress reconstruction was completed using slicken line measurements from striated surfaces in the Drumlummon mine. A total of 29 striated surfaces were measured in the mine with some of the surfaces containing both a younger and older set of striations. The analysis of the youngest set of striations gave principal stress axes of σ_1= 86→002, σ_2= 02→116 and σ_3=04→207 (Figure 22). A paleostress field was then derived in the T-TECTO program using the Right Dihedra Method (Angelier & Mechler, 1977). The result is presented in P and T quadrants roughly agreeing with a normal fault setting. The paleostress reconstruction result is comparable to the P and T quadrants from a 1973 earthquake study (Freidline, Smith, & Blackwell, 1976) done in the the MMD. Both the results from the paleostress analysis on the younger striations and the 1973 earthquake study show a normal fault setting with the minimum stress direction orientated northeast-

southwest. The paleostress analysis was also completed on the older set of striations. The results show the older striations principal stress axes of σ_1=12→295, σ_2=23→200, and σ_3=63→051 (Figure 22). The results for the older striations are not considered robust because only six striations were used instead of the nine recommended by Orife and Lisle (2006). However, even with the small sample size the older striations still provide useful results for comparison.

DISCUSSION

Geochronology

One of the major contributions of this study is that Re/0s dates for molybdenite mineralization show two different episodes of mineralization in the Drumlummon and Bald Butte systems, at ~80 Ma and ~40 Ma respectively. These age dates coincide temporally with the previously identified intrusive events in the MMD: the Marysville stock at ~80 Ma and the Bald Butte, Silver City, and Empire intrusives at ~42-39 Ma. Although plutons of both ages have long been recognized, the most recent work in the MMD has attributed mineralization only to the Eocene events (Walker, 1992a, Knopf, 1950b) in contrast to the Barrel (1907) interpretation of gold mineralization being related to the Marysville stock. Knopf (1950) disproved the theory of gold in the Drumlummon mine being related to the Marysville stock using crosscutting relationships. The crosscutting relationships in the Drumlummon mine were consistent with gold mineralization being Eocene in age. Later radiometric age dating would prove that other gold and molybdenum mineralization in the MMD is Eocene in age (Walker, 1992b, Knopf, 1950a). The newly discovered Cretaceous molybdenite mineralization in the Drumlummon mine is temporally and spatially related to the Marysville stock. The ~80 Ma age date of the molybdenite mineralization means that mineralization would have occurred at a depth of roughly 4 km based on fluid inclusion work (Petefish, 1975). Porphyry systems typically form in the upper 4 km of the Earth's crust (Singer et al., 2008). To

date, none of the workings or drilling in the Drumlummon mine have discovered a deeper porphyry. The lack of evidence for a deeper porphyry suggests that the molybdenite mineralization may have been sourced from the Marysville stock. The recognition of possible molybdenite mineralization related to the Marysville stock suggests that a related porphyry system may have been located above the stock. Perhaps precious metal-bearing veins that would have been emplaced on top of the system (Sillitoe & Hedenquist, 2003) had been eroded, leaving molybdenite-bearing veins at current exposure levels. Speculatively, extensive placer deposits in the Silver City drainage and Helena Valley could partly be related to such an eroded system. The felsic dikes mapped in the Drumlummon mine are also interpreted to be part of the Marysville stock system.

Eocene mineralization is seen throughout the MMD. Examples include the Drumlummon gold system (Knopf, 1950) and the Bald Butte molybdenum porphyry system (Chapter 5). The similar ages for the molybdenite mineralization at Bald Butte and the underlying porphyry provide further evidence for a connection between the two. The ages coupled with the alteration seen at Bald Butte provide strong evidence that the Bald Butte pluton is the source of molybdenite mineralization at Bald Butte. The Eocene Drumlummon gold mineralization fits with other gold deposits in the MMD (Walker, 1992a). The Eocene age dates correspond with the ~40 Ma intrusive events seen throughout the district. The corresponding ages provide evidence for the relation between the plutons and precious-metal mineralization in the district.

Deposit Model of The Drumlummon Mine

The Eocene-age gold system in the Drumlummon mine is most consistent with an intermediate sulfide epithermal gold system (Hedenquist et al., 1996). This is supported by several lines of evidence including: (1) gangue mineral assemblage, (2) sulfide abundance and species, (3) alteration minerals, (4) major and minor metals, and (5) ore textures. Some of the criteria seen at the Drumlummon mine are consistent with multiple models, such as quartz being a gangue mineral (seen in all intrusive related gold systems). However, all observations in the Drumlummon mine only match all five criteria of an intermediate sulfide epithermal gold system (Table 4, at end of Chapter Two).

Sulfide species and abundance provide robust ways to define a deposit model. Sulfide species of sphalerite, acanthite-argentite, chalcopyrite, and galena can be present in either low or intermediate sulfidation epithermal systems (Table 4). However, the high amount of sphalerite favors an intermediate sulfidation system (Sillitoe & Hedenquist, 2003). Further, the Einaudi et al. (2003) (Figure 11, at end of Chapter Two) criterion can also be used to differentiate the different types of epithermal systems based on sulfide species. Based on Einaudi et al. (2003) the presence of chalcopyrite is consistent with an intermediate sulfidation system. The less than 1 percent sulfide abundance in the ore veins is consistent with a low sulfidation or pluton related system. However, recent work has noted the presence of possible high-grade feeder veins containing high sulfide abundance (Ben Porterfield, personal communication). The sulfide abundance in the high-grade

feeder veins at the Drumlummon mine are consistent with an intermediate sulfidation epithermal deposit. The low-sulfide abundance in the mineable ore veins at the Drumlummon mine could result from the mineable ore veins containing gangue minerals from both non-mineralizinged and mineralizing fluid pulses, while the sulfide abundance in the high-grade feeder veins only contain products of mineralizing events.

Presence of major and minor metals also provides a means to differentiate ore deposit models since metal concentrations will vary with each deposit type. Ag and Au are main metals in the Drumlummon mine and the ratio of Ag to Au (Table 1, Table 2, at end of Chapter One) is high. Base metals (Zn, Pb, and Cu) were also identified as main metals in the Drumlummon mine (Table 1). Data for minor metals was only available for the Charly vein showing As and Sb as minor metals. Both the major and minor metals associated with gold at the Drumlummon mine are most consistent with an intermediate sulfide epithermal system. The metals present in a deposit can also be used to infer the magma source that caused the mineralization (Ishihara, 1981) (Figure 23). The metals present in the Drumlummon mine suggest derivation from a magnetite-type magma (Figure 23). The formation of a magnetite-series magma generally takes place under oxidized plutonic conditions common in forearc settings (Ishihara, 1981).

Gangue minerals and ore body formed in gold deposits are partially related to fluid sourcing and formation temperature. Thus, they will vary according to the deposit type. Silica gangue could be found in all the gold deposit models (Table 4).

However, carbonate and barite gangue minerals are only found in high-, intermediate-, and low-sulfide epithermal deposits. However, the local presence of barite in the Drumlummon mine is most consistent with an intermediate- or low-sulfide epithermal deposit. The Drumlummon ore is located in veins as is characteristic of epithermal, pluton-related, or orogenic systems. Mapping of the 400' level of the Drumlummon mine showed extensionive brecciation related to the veins (Plate A in Appendix F). This is also indicative of an epithermal system. While the ore form at Drumlummon can occur in three different deposit models when used with the gangue minerals the Drumlummon ore veins are most consistent with a low- or intermediate-sulfide epithermal deposit.

The alteration minerals in ore deposits vary for reasons similar to gangue minerals. Country rocks throughout the 400-level of the Drumlummon mine are located immediately southwest of the Marysville stock and have been metamorphosed to hornfels (Rice, 1977). The hornfels has been interpreted to be related to the intrusion of the Marysville stock during the Cretaceous (Baagsgaard, Folinsbee, & Lipson, 1961b, Rice, 1977). Mineralized gold veins and alteration overprint the hornfels demonstrating that they occurred after this Cretaceous metamorphic event. Thus, the hornfels predates and is probably not related to the gold mineralization located in the Drumlummon mine and mineralization occurred after the Cretaceous. Argillic (clay) and chlorite alteration is found together and is related to the Drumlummon gold mineralization and is typically found in high-, intermediate-, or low-sulfidation epithermal and porphyry gold deposit models

(Table 4). However, the presence of clays and chlorite together is indicative of neutral to alkaline pH fluids (Figure 24). Neutral to alkaline pH fluids suggest that mineralizing fluids were not magmatic, thus ruling out high-sulfidation and porphyry deposits. The alteration minerals suggest a low- or intermediate-sulfidation epithermal system.

Control on Ore Veins at the Drumlummon Mine

Ore in the Drumlummon mine was determined to be structurally controlled, rather than hydrothermally or lithologically controlled. Two separate criteria, ore body geometry (Sillitoe, 1993) and ore deposit grade (Hedenquist et al., 2000), were used to determine the control on the ore. The lack of residual vuggy silica in ore veins argues against the possibility of the ore veins being hydrothermally controlled (Sillitoe, 1993). Furthermore, the veins cut across bedding planes in the country rock. According to the Sillitoe (1993) criteria, veins cutting across the bedding planes suggest limited lithologic control on the ore veins. The thickness, orientations, and spacing of ore veins are consistent with a vein swarm (Figure 13, at end of Chapter Three). The vein-swarm form of ore in the Drumlummon mine and the lack of evidence for lithologic or hydrothermal control suggest that the veins were structurally controlled according to the Sillitoe (1993) criteria.

The ore grade from the Drumlummon mine is consistent with a high-grade (structurally controlled) deposit. The historic average grade for the Drumlummon mine plots near the lower limit of economic deposits and does not plot in any of the

zones outlined by the Hedenquist et al. (2000) chart (Figure 14, at end of Chapter Three). However, on the Y-axis the Drumlummon average-grade ore plots with other high-grade (structurally controlled) deposits; the area in which the Drumlummon average-grade ore plots would likely be in the high-grade (structurally controlled) zone if the chart included deposits with the lower tonnages seen at Drulmummon. The historic high-grade Drumlummon ore plots well within the zone for a structurally controlled ore deposit (Figure 14). The historic ore grades have been confirmed by RX Exploration's recent work in the Drumlummon mine (Table 2). Thus, the Drumlummon deposit is consistent with a high-grade (structurally controlled) deposit using the Hedenquist et al. (2000) criteria.

Structural Control on Ore Veins at the Drumlummon Mine

Fracture data from surface outcrop mapping and underground mapping shows that fracture control is a likely focusing process in the Drumlummon mine. Outcrops in the C domain are above the Drumlummon mine and were used in the fracture control analysis. The dominant fracture set in the C domain is orientated northeast-southwest and is similar to the orientation of ore veins and fractures in the Drumlummon mine. The minor west-northwest-east-southeast-orientated fracture set in the C domain was also noted underground in the Drumlummon mine. These fracture sets have a similar orientation to the Northstar vein in the Drumlummon mine. The main and minor fracture sets have a similar orientation to

the ore veins suggesting that fractures were a focusing process for vein emplacement.

The fracture sets in other domains throughout the district also show similar orientations to the gold veins in the corresponding domain (Figure 6, Figure 18). The major east-northeast fracture set in both the A and B domains has the same orientation as gold veins located in those domains. The general correspondence of gold vein and fracture orientation in the different domains suggests a strong structural control on ore veins. Given this, the surface fractures should provide a good indicator of gold vein orientations in the subsurface throughout the MMD.

Deformational History in the MMD

The deformational and intrusive episodes observed in the MMD show an apparent transition from transpression to transtension on the LCL, followed by later Basin and Range-style deformation (Figure 25, Figure 24). Orientations of the earliest structures and intrusives follow predicted transpressional orientations. A middle stage of deformation with a predicted east-west principal stress was discovered during the mapping. The youngest structures and intrusives mapped follow structural orientations predicted for transtension on the LCL or Basin and Range-style deformation. The orientation and timing of structures in the MMD support the idea that deformation related to regional stress fields occurred in the MMD.

Structures interpreted to have been caused by transpression on the LCL were mapped throughout the MMD (Figure 24). The predicted transpressional stress field in the LCL had a maximum principal stress ($\sigma 1$) direction aligned northeast-southwest (Figure 25). Normal faults, major fracture, and vein sets that formed during transpression would strike parallel to the predicted northeast-southwest principal stress direction. The minor fracture set in the Marysville stock and major fracture sets in the C, D, and E domains in the MMD have this northeast-southwest orientation. The ~80 Ma intrusion of the Marysville stock provides an upper limit on the age of structures within the stock. The subordinance of the northeast-southwest fractures in the stock could be because the transpressional stress field would be short lived after emplacement of the stock. The oldest veins and normal faults mapped underground in the Drumlummon mine also followed the predicted transpressional maximum principal stress direction (Figure 20). This is also true of veins interpreted to be older based on crosscutting relationships at Bald Butte (Appendix E). While the stockwork veining at Bald Butte is constrained by Re/Os age dating at 39.9 Ma (Table 5), the sequence to the stockwork veins suggests that the veins first followed the major northeast-southwest fracture set created during transpression (Appendix E). P shears predicted during transpression would strike to the southeast-northwest and Riedel shears predicted during transpression would be predicted to strike to the southwest-northeast (Figure 25). Evidence for the development of both P and Riedel shears is seen in the Drumlummon mine with the southeast-striking veins the same as the predicted P shears. Support for the Riedel

shearing process is seen in the right lateral strike-slip faults in the Drumlummon mine that have geometries and kinematics similar to thee predicted Riedel shears developed during transpression. Structures related to transpression on the LCL were observed in all three mapping locations in the MMD.

Evidence for a newly discovered period of deformation between the transpression and transtension periods was noted throughout the MMD. This deformational period is observed to have east-west striking structures. At the Drumlummon mine, the stage 4, east-west oriented, normal faults are assumed to have occurred during this deformational period. This newly recognized deformation period is also seen at Bald Butte with the middle stage of east-west veining. The orientation of faults and veins during this deformational period suggests that its maximum principal stress direction was orientated vertically and its minimum principal stress direction was orientated north-south. The cause of this stress geometry may be a local event.

Transtensional structures with a predicted maximum principal stress orientated northwest-southeast occurred last (Figure 25). Although the age of the oldest striated surfaces in the Drumlummon mine is not constrained, and there is a small sample size, the calculated paleostress field (Figure 21) is consistent with the predicted transtensional stress field (Figure 25). During transtension, predicted normal faults, major fracture sets, and vein sets would strike with the northwest-southeast principal stress direction. Evidence for this can be seen in the final stage of veining and faulting at Bald Butte (Appendix E), as well as fracture patterns in the

majority of the domains throughout the district (Figure 18). The dominance of the northwest-southeast oriented fractures over the northeast-southwest oriented fractures in the Marysville stock suggests that the transtensional stress field was active longer than transpression after the emplacement of the stock at ~80 Ma. In B domain the lack of the northwest-southeast fracture may be because the northwest-southeast striking anticline was first formed during transpression, to be later domed during transtension. As a result, local fractures developed perpendicular to the axis of the anticline during transtension. The east-west right lateral strike-slip fault could be caused by normal fault reactivated during the transtension. Riedel shears striking to the northeast would have occurred during transtension (Figure 25). Evidence for this is seen in the late left lateral strike-slip faults in the Drumlummon mine. The structures in the Drumlummon mine, MMD fractures patterns, Bald Butte veins, and faults provide evidence for the formation of transtension-related structures throughout the MMD.

Predicted orientations of some structures would not change with the transition from transtension to Basin and Range styles in the MMD. However, the maximum principal stress orientation would change from horizontal northeast-southwest to a vertical direction. This change in stress field was observed in the paleostress reconstruction. As stated earlier, the oldest set of minor fault striations yielded a stress field consistent with transtension on the LCL. The youngest set of striations in the paleostress analysis yielded a vertical maximum principal compressional stress and a northwest-southeast maximum principal stress (Figure

21D). This stress field is similar to the current stress field as indicated by current local earthquake focal mechanisms (Freidline et al., 1976) that reflect Basin and Range styles (Lageson & Stickney, 2000).

Evolution of the Au Veins in the Drumlummon Mine

The development of gold veins in the Drumlummon mine consisted of two main stages (Figure 26). Early structures developed that would later control vein emplacement by providing a conduit for later mineralizing fluids to follow. The structures that controlled vein emplacement were in the form of fractures and faults, as discussed in previous sections. The vein controlling fractures and faults were developed during transpression occurring before ~50 Ma in the MMD (Figure 24).

Gold mineralization in the Drumlummon mine has been determined to be from an intermediate-sulfide epithermal system occurring at ~40 Ma (Knopf, 1950a). The age and composition of the Silver City stock suggests it to be the source of mineralization in the Drumlummon mine (Figure 26). In order for mineralizing fluids from the Silver City stock to be transported to the Drumlummon ore veins they would have to have first followed lithologic contacts moving west towards the Marysville stock. The high-grade feeder veins discovered by RX Exploratoin provide evidence that fluids could have been transported in this fashion. Once the fluids reached the preexisting structures close to the stock they followed them and formed the ore veins in the Drumlummon mine. The discovery of possible feeder veins east

of the Drumlummon mine by RX Exploration supports this theory. The position of the Marysville stock may have also provided lithologic controls secondary to the structural controls.

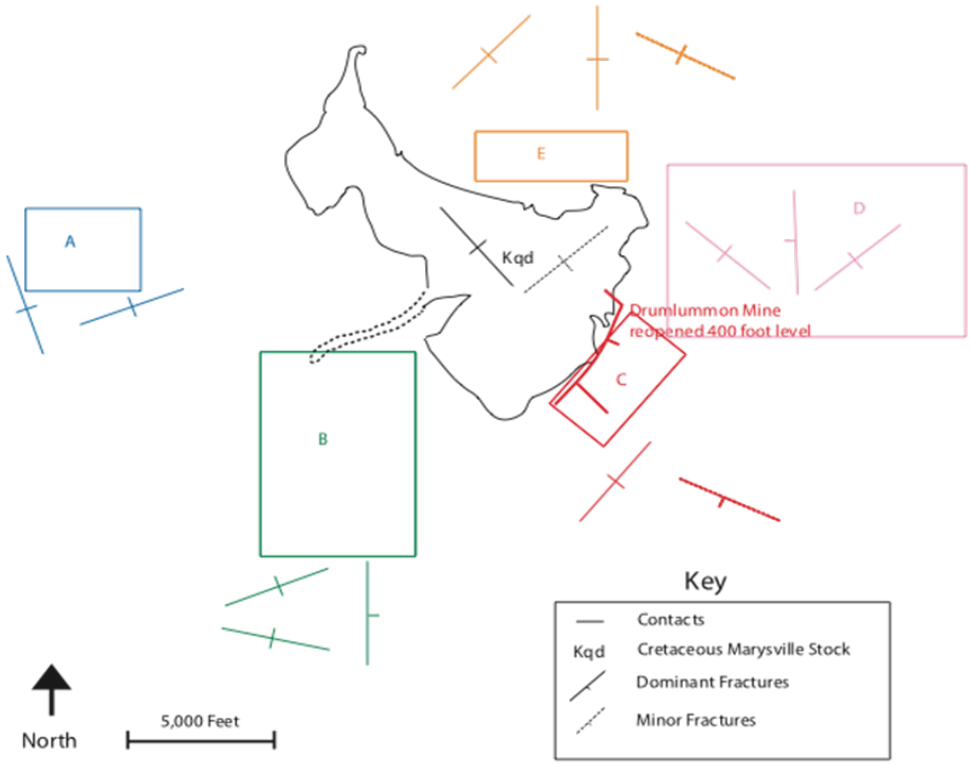

Figure 18: Major and minor fracture patterns in the MMD broken into structural domains. The colored boxes show the area of each domain, the domains are labeled with letters that correspond in color. Chapter Five, Appendix C.

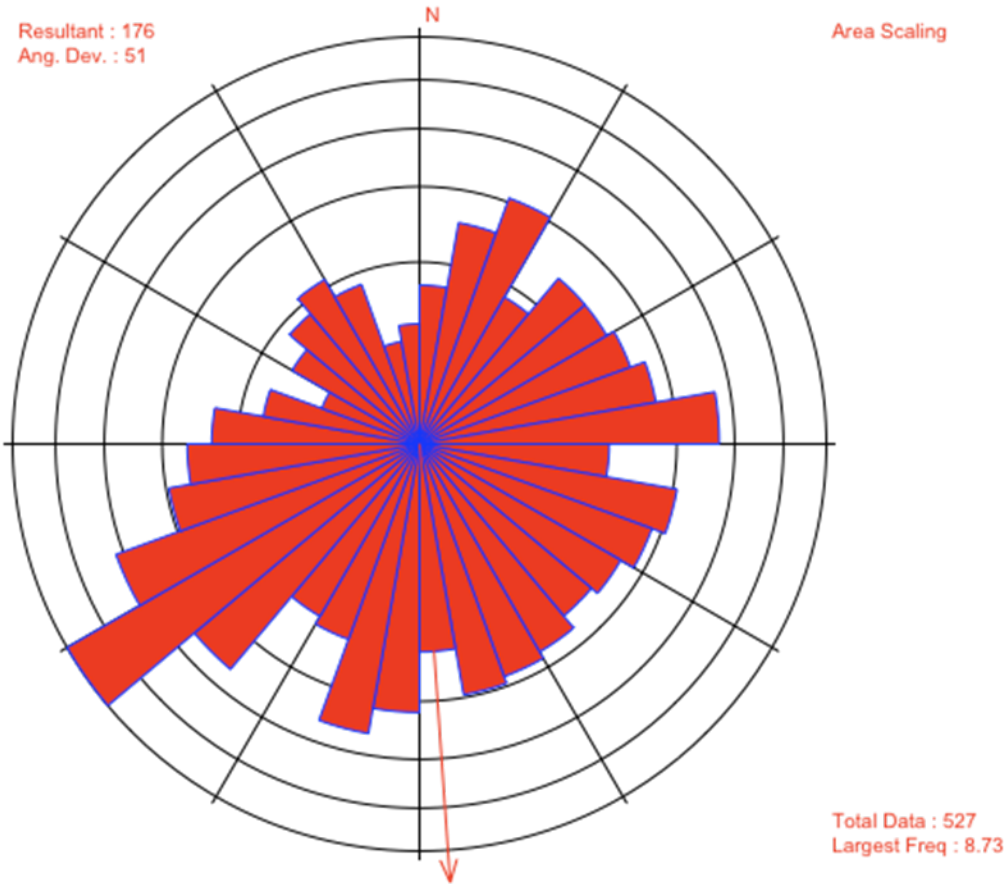

Figure 19: Rose diagram summarizing all vein strikes measured within the Bald Butte mapping area. Three sets of veins are prevalent in the map area listed in order of abundance: (1) Steeply dipping southwest-striking veins (2) Steeply dipping southeast-striking veins (3) Steeply dipping east-west-striking veins. Chapter Five, Appendix D.

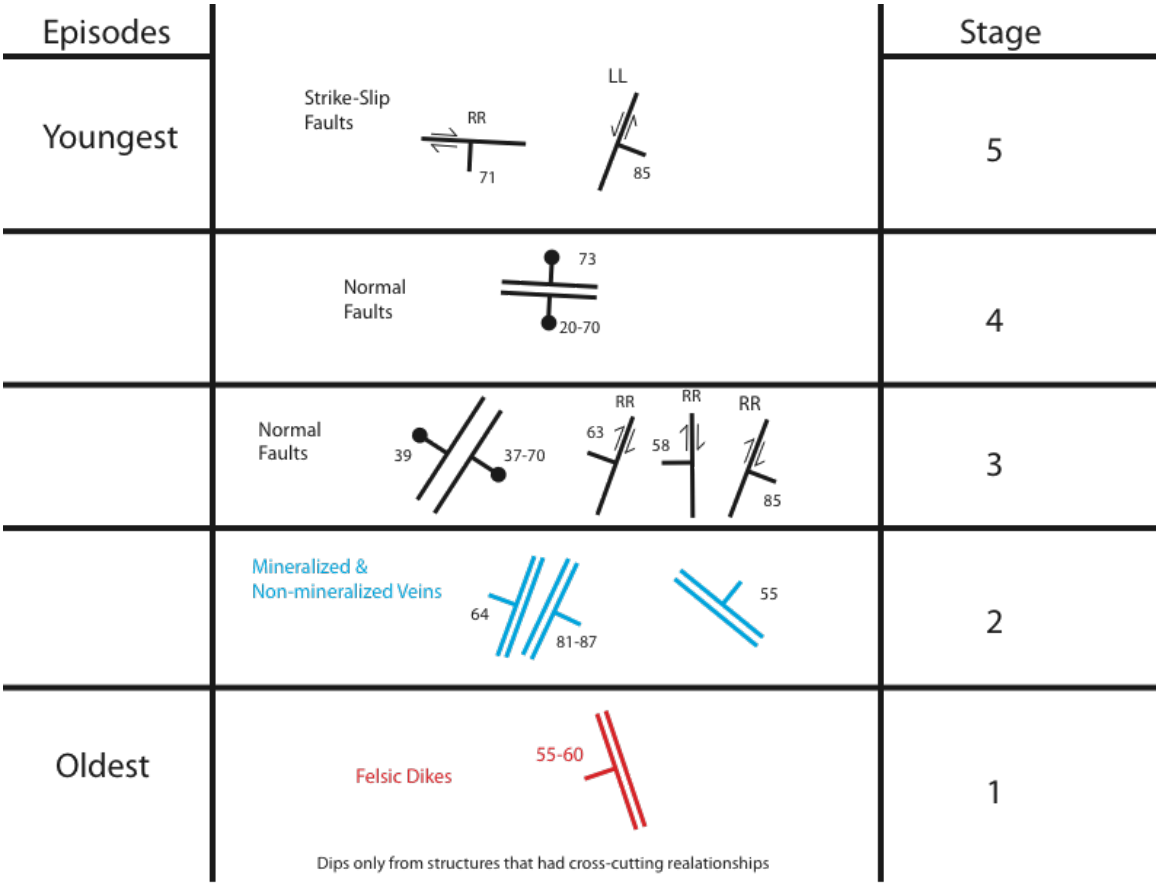

Figure 20: Four stages of structural events including Dikes, Veins, Gouge Zones, Faults, and other Structures mapped in the 400-foot level of the Drumlummon Mine. From oldest to youngest the events are (1) Intrusion of Felsic Dikes, (2) Mineralized Veins (primarily qz+carb) (3) Oldest stage of normal faults (4) Youngest stage of normal faults (5) Strike-slip faults. Chapter Five.

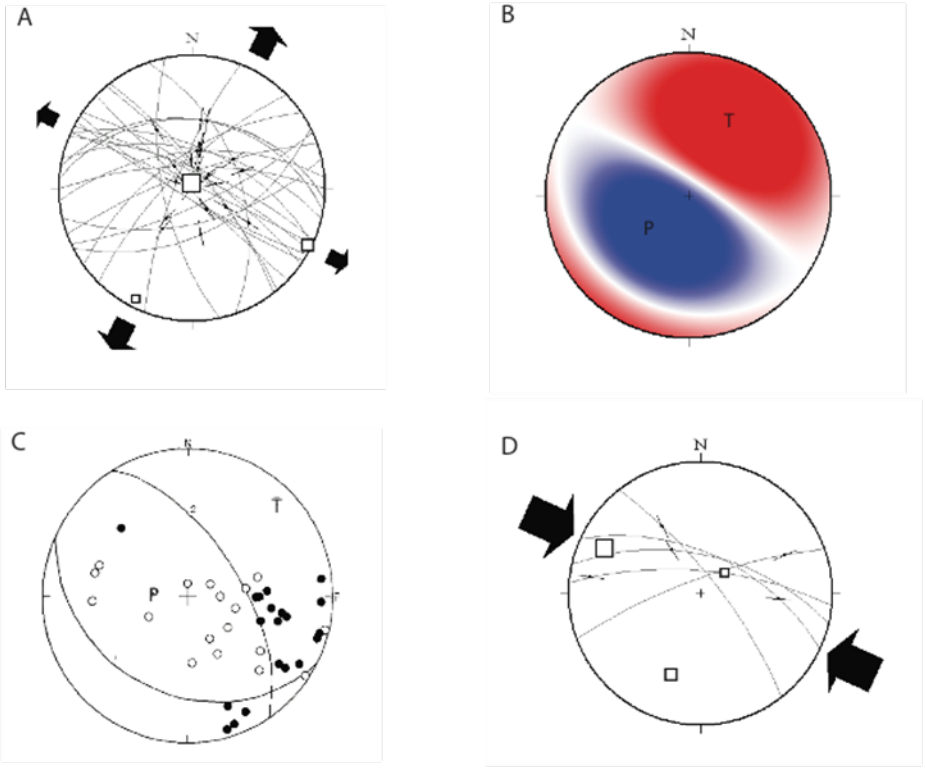

Figure 21: Paleostress analysis results from the T-TECTO program (Zalohar & Vrabec, 2007, Chapter Five). The striated fractures measurements were from the 400-foot level of the Drumlummon mine; roughly 30 measurements were taken. A: Principal stress directions of the youngest set of striations from the Mohr-Navier shear failure criterion method. Open squares show the direction of principal stress axes σ_1= 86→002, σ_2= 02→116, σ_3= 04→207. Black arrows show the relative magnitude of strain in the horizontal plane. B: Visualization of the P and T quadrants and fields using the right Dihedra Method (Angelier & Mechler, 1977) in the T-TECTO program (Zalohar & Vrabec, 2007). Blue – P quadrants, Red - T quadrants. The results are similar to results from a field study (Freidline et al., 1976; Part C) conducted in the area. C: P and T quadrants and fields from a 1973 earthquake study (Freidline et al., 1976). Fault plane solutions indicate normal faulting with a P axis of 271/71W and a T axis of 045/14NE. D: Principal stress directions of the oldest set of striations from the Mohr-Navier shear failure criterion method. Direction of principal stress axes σ_1= 12→295, σ_2= 23→200, σ_3= 63→051.

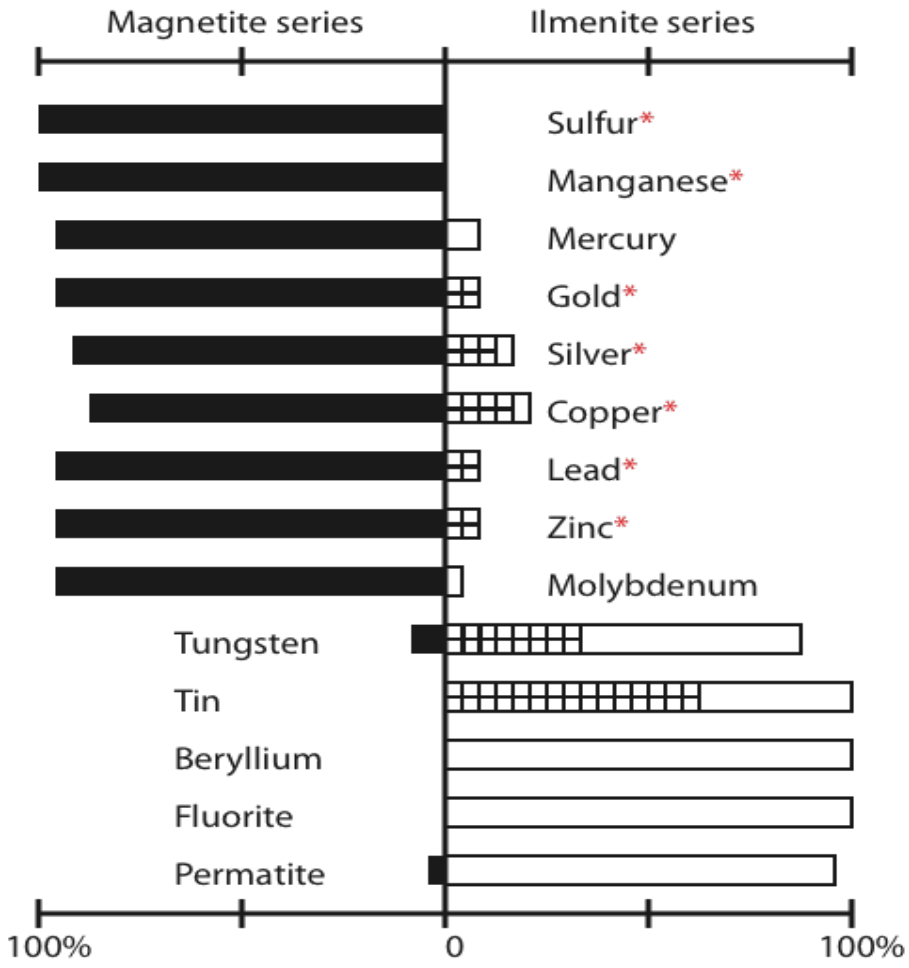

Figure 22: Ratios of ore components precipitated in ore deposits as classified in terms of the magnetite series and ilmenite series. Solid bars represent ores from the magnetite series granitic terrains; shaded bars represent weakly magnetic magnetite series terrains; white bars represent ilmenite series terrains. Red asterisk denotes metals associated with gold mineralization in the Drumlummon mine. Modified from Ishihara, 1981, Chapter Five.

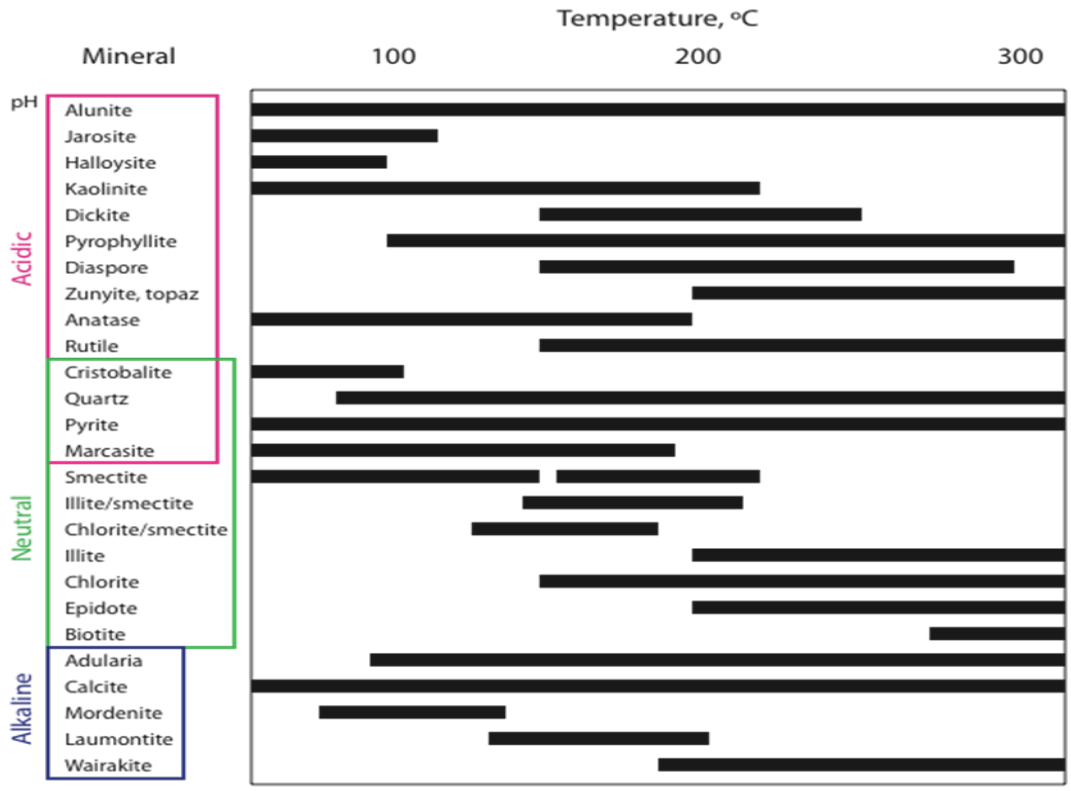

Figure 23: Graph showing temperature stability of hydrothermal minerals common in epithermal environments, arranged by their stability with respect to pH. From Hedenquist et al., 1996.

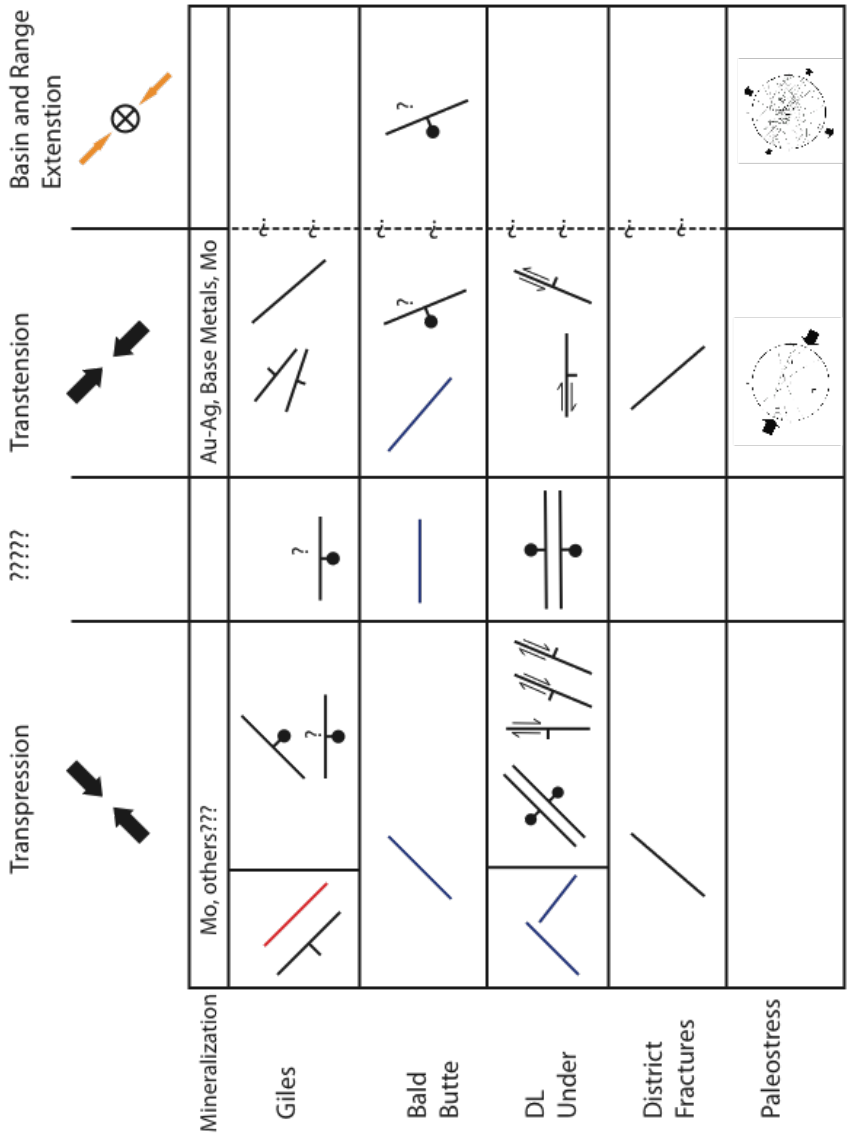

Figure 24: Deformational history of the MMD. Compiled from Walker, 1992; Chapter Five.

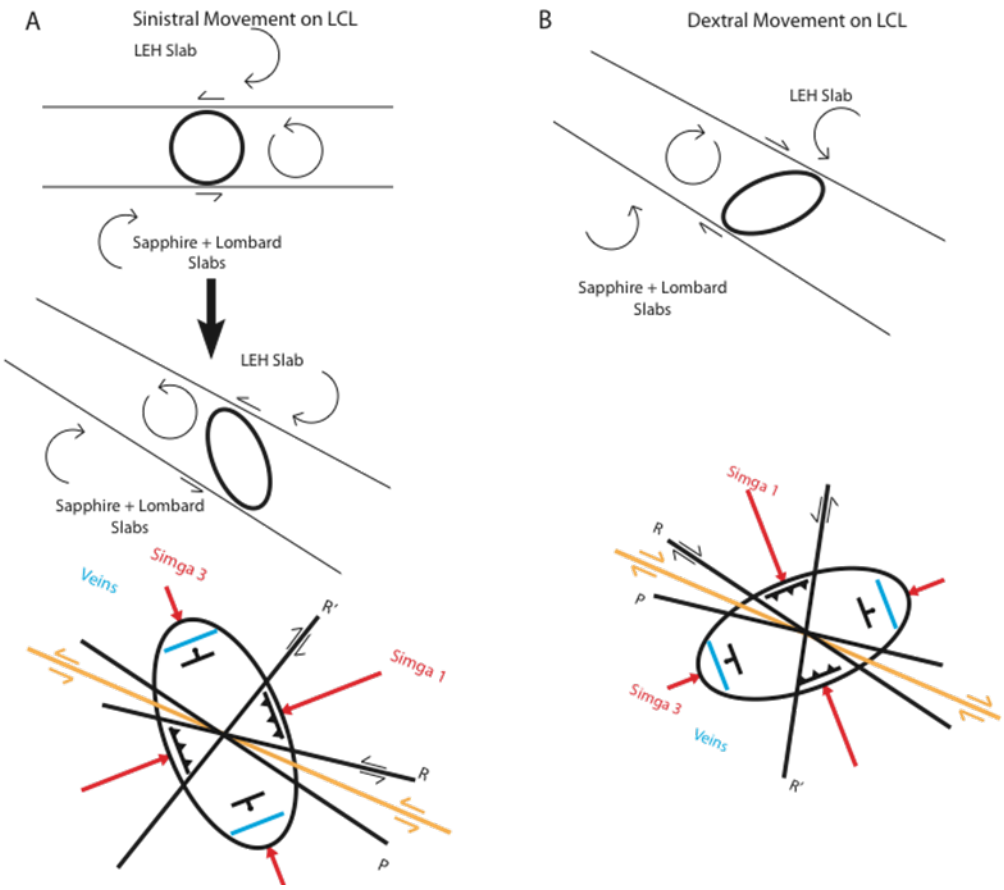

Figure 25: Model showing (A) the evolution of transpressional simple shear in the LCL and related stress field and (B) after collapse of fold-and-thrust belt transtension on LCL and related stress field. From Sears and Hendrix, 2004.

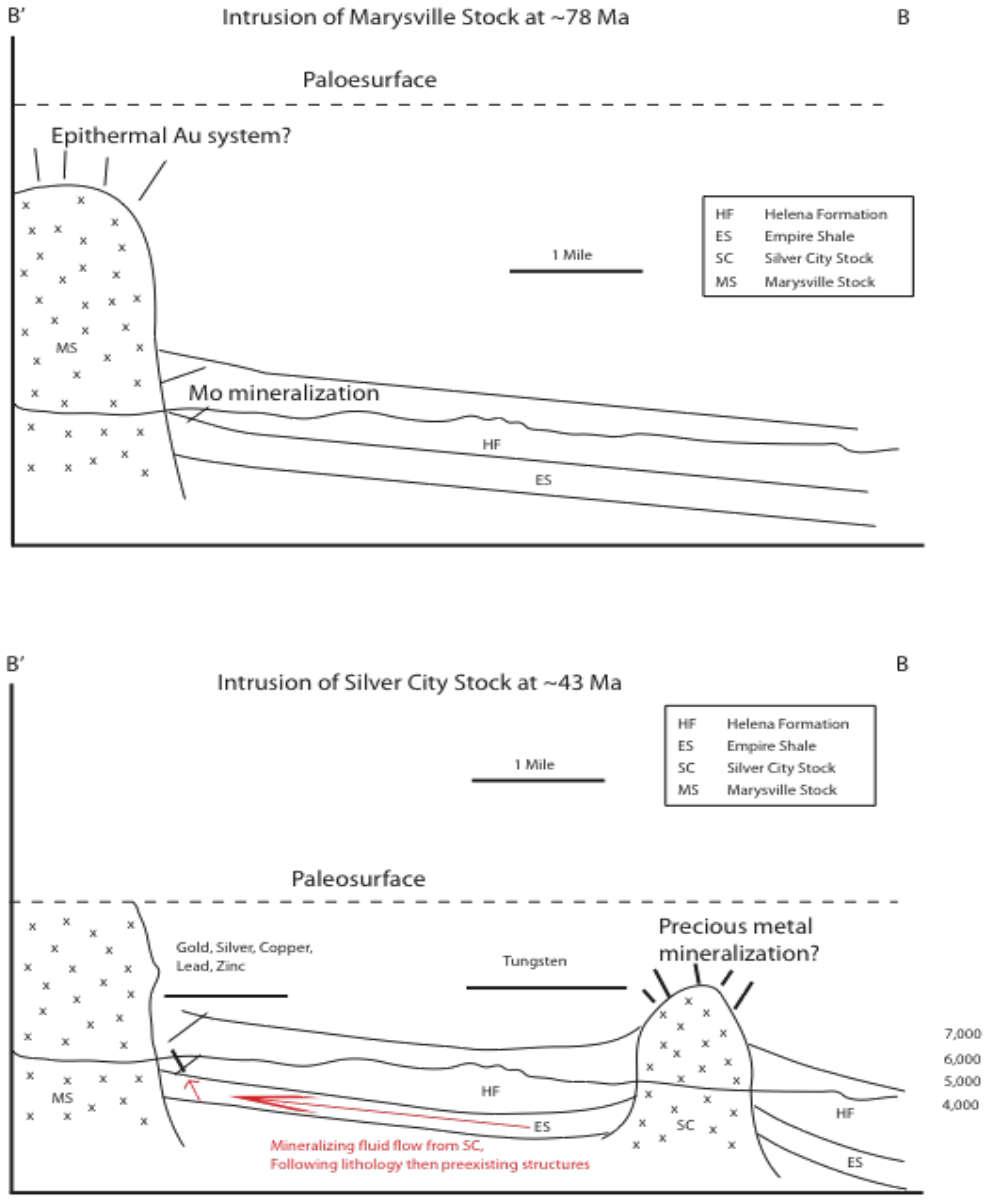

Figure 26: Possible evolution of ore veins in the Drumlummon mine. Chapter Six.

Table 5: Re-Os age dates, Carius tube dissolution with Double Os spike on 40 mg of molybdenite and all errors are 2-sigma level.

AIRIE run	Sample Location	Re, ppm	^{187}Os, ppb	Age, Ma
MD-1156	Drumlummon Mine	205 (1)	171.1 (2)	79.6 $\pm$ 0.6
MD-1158	Bald Butte	0.2644 (2)	0.1104 (1)	39.9 $\pm$ 0.1

Table 6: Table summarizing precious and base metal minerals in the Christmas, Castleton, Drumlummon, and Charly veins. Chapter Five.

Vein	**Precious Metal Minerals**	**Base Metal Minerals**
Christmas	None	Galena - PbS
		Sphalerite – (Zn,Fe)S
Castleton	Acanthite-argentite – AgS_2	Chalcopyrite - $CuFeS_2$
	Chalcopyrite with silver – $CuFeS_2$ with Ag	Galena - PbS
	Jalpaite – Ag_3CuS_2	Sphalerite – (Zn,Fe)S
	Stromeyerite - AgCuS	Tetrahedrite - $(Cu,Fe)_{12}Sb_4S_{13}$
	Freibergite – $Cu_{12}Sb_4S_{13}$ with Ag	
Drumlummon	Chalcopyrite with silver – $CuFeS_2$ with Ag	Chalcopyrite – $CuFeS_2$
	Stromeyerite - AgCuS	Galena - PbS
	Silver copper sulfide – Ag_7CuS	Sphalerite – (Zn,Fe)S
	Acanthite-argentite – AgS_2	

Table 6 - Continued

Vein	**Precious Metal Minerals**	**Base Metal Minerals**
Drumlummon	Native copper with minor sulfur and silver – Cu with S and Ag	
Charly	Chalcopyrite with silver – $CuFeS_2$ with Ag	Sphalerite – (Zn,Fe)S
	Sphalerite with silver – (Zn,Fe)S with Ag	
	Pyrite with silver – FeS with Ag	
	Argyropyrite - $Ag_2Fe_7S_{11}$	
	Stromeyerite - AgCuS	
	Acanthite-argentite –AgS_2	
	Silver zinc sulfide – Ag_3ZnS_3	
	Silver sulfide - AgS	

CONCLUSIONS

- Two distinct episodes of plutonism and mineralization are recorded in the MMD. The first phase occurred at ~80 Ma with intrusion of the Marysville stock and molybdenite mineralization in the Drumlummon mine. The second phase occurred at ~40 Ma with multiple mineralizing intrusions in the MMD including gold mineralization in the Drumlummon mine and gold, silver, and molybdenum mineralization associated with theBald Butte pluton.
- The gold-bearing veins located in the Drumlummon mine are part of an Eocene aged, intermediate-sulfidation, epithermal gold system.
- The Silver City stock (a magnetite-type granite) may be the mineralization source for the Drumlummon mine.
- Fracture control is a form of structural control in the Drumlummon mine.
- A deformational history in the MMD recorded transpressional structures that were overprinted by transtensional structures. East-west orientated structures were documented between the transpressional and transtensional structures.

REFERENCES CITED

Angelier, J. (1979) Determination of the Mean Principal Directions of Stresses for a Given Fault Population. *Tectonophysics,* 56**,** T17-T26.

--- (1989) From Orientation to Magnitudes in Paleostress Determinations using Fault SRIENTATION TO MAGNITUDES IN PALEOSTRESS DETERMINATIONS USING FAULT SLIP DATA. *Journal of Structural Geology,* 11**,** 37-50.

Angelier, J. & P. Mechler (1977) Sur une methode graphique de recherche des contraintes principales egalement utilisables en tectonique et en seismologie : la methode des diedres droits. *Bulletin de la Societe Geologique de France,* 19**,** 1309-1318.

Armstrong, R. L. (1968) Sevier orogenic belt in Neveda and Utah. *Geological Society of America Bulletin,* 79**,** 429-458.

Armstrong, R. L., V. F. Hollister & J. E. Harakel (1978) K-Ar dates for mineralization in the White Cloud-Cannivan porphyry molybdenum belt of Idaho and Montana. *Economic Geology,* 73**,** 94-96.

Atwater, T. (1970) Implications of plate tectonics for the Cenozoic tectonic evolution of western North America. *Geological Society of America Bulletin,* 81**,** 3513-3535.

Baagsgaard, H., R. E. Folinsbee & J. Lipson. 1961a. Potassium-argon dates for Cordilleran granites. 689-702. Geological Society of America Bulletin.

--- (1961b) Potassium-argon dates for Cordilleran granites. 689-702.

Barrell, J. 1907. Geology of the Marysville mining district, Montana; a study of igneous intrusion and contact metamorphism. 178. U. S. Geological Survey Professional Paper.

Bingen, B. & H. J. Stein (2003) Molybdenite Re-Os dating of biotite dehydration melting in the Rogaland high-temperature granulites, S Norway. *Earth Planet Sci Lett,* 208**,** 181-195.

Blackwell, D. D., B. C. A., T. T. Goforth, M. J. Holdaway, P. Morgan, D. Petefish, T. Rape, J. L. Steele, R. E. Spafford & A. F. Waibel. 1974. A brief description of geological and geophysical exploration of the Marysville geothermal area. 98-110. Conference on Research for the Development of Geothermal Energy Resources (see Nakamura, Yukio); Resources exploration and assessment.

Bott, M. H. P. (1959) The Mechanics of Oblique Slip Faulting. *Geological Magazine,* 96**,** 109-117.

Cline, J. S., A. H. Hofstra, J. L. Muntean, R. M. Tosdal & K. A. Hickey. 2005. Carlin-Type Gold Deposits in Neveda: Critical Geologic Characteristics and Viable Models. In *Economic Geology: One Hundredth Anniversary Volume,* eds. J. W. Hedenquist, J. F. H. Thompson, R. J. Goldfarb & J. P. Richards, 451-484.

Coney, P. J. & S. J. Reynolds (1977) Cordilleran Benioff zones. *Nature,* 270**,** 403-406.

Constenius, K. N. (1996) Late Paleogene extensional collapse of the Cordilleran foreland fold and thrust belt. *Geological Society of America Bulletin,* 108**,** 20-39.

Coulomb, C. A. (1776) Sur une application des regles maximis et minimis a quelques problemes de statique a l'architecture. *Academie Royale des Sciences: Histoire et Memoires de Mathematique et de Physique,* 7**,** 57-60.

DeCelles, P. G. 2004. Late Jurassic to Eocene evolution of the Cordilleran thrust belt and foreland basin system, western U.S.A., 105-168. American Journal of Science.

Dickinson, W. R. 2004. Evolution of the North American Cordillera. 13-45. Annual Review of Earth and Planetary Sciences.

Evans, K. V., J. N. Aleinikoff, J. D. Obradovich & C. M. Fanning (2000) SHRIMP U-Pb geochronology of volcanic rocks, Belt Supergroup, western Montana: evidence for rapid deposition of sedimentary strata. *Canadian Journal of Earth Sciences,* 37**,** 1287-1300.

Fleischer, M. (1955) Minor Elements in Some Sulfide Minerals. *Economic Geology***,** 970-1024.

Foster, D. A., P. T. Doughty, T. J. Kalakay, C. M. Fanning, C. Samuel, W. C. Grice & J. Vogl. 2007. Kinematics and timing of exhumation of metamorphic core complexes along the Lewis and Clark fault zone, northern Rocky Mountains, USA. In *Exhumation Associated with Continental Strike-Slip Fault Systems,* eds. A. B. Till, S. M. Roeske, J. C. Sample & D. A. Foster, 207-232. Geological Society of America Special Paper.

Foster, D. A., C. Schafer, C. M. Fanning & D. W. Hyndman (2001) Relationships between crustal partial melting, plutonism, orogeny, and exhumation: Idaho-Bitterroot batholith. *Tectonophysics,* 342**,** 313-350.

Freidline, R. A., R. B. Smith & D. D. Blackwell. 1976. Seismicity and Contemporary Tectonics of the Helena, Montana Area. In *Bulletin of the Seismological Society of America*, 81-95.

Goldfarb, R. J., T. Baker, B. Dube, D. I. Groves, C. J. R. Hart & P. Gosselin. 2005. Distribution, Character, and Genesis of Gold Deposits in Metamorphic Terranes. In *Economic Geology One Hundredth Anniversary Volume,* eds. J. W. Hedenquist, J. F. H. Thompson, R. J. Goldfard & J. P. Richards, 451-484.

Goldfarb, R. J., D. I. Groves & S. Gardoll (2001) Orogenic gold and geologic time: a global synthesis. *Ore Geology Reviews,* 18**,** 1-75.

Harrison, J. C. & A. W. Bally. 1988. Cross-sections of the Parry Islands fold belt on Melville Island, Canadian Arctic Islands; implications for the timing and kinematic history of some thin-skinned decollement systems. 311-332. Bulletin of Canadian Petroleum Geology.

Hedenquist, J. W., A. Arribas & E. Ganzalez-Urien (2000) Exploration for Epithermal Gold Deposits. *SEG Reviews,* 13**,** 245-277.

Hedenquist, J. W., E. Izawa, A. Arribas & N. C. White (1996) Epithermal gold deposits: Styles, characteristics, and exploration. *Resource Geology Special Publication,* 1**,** 16.

Hodges, K. V. & J. D. Applegate (1993) AGE OF TERTIARY EXTENSION IN THE BITTERROOT METAMORPHIC CORE COMPLEX, MONTANA AND IDAHO. *Geology,* 21**,** 161-164.

House, M. A., S. A. Bowring & K. V. Hodges (2002) Implications of middle Eocene epizonal plutonism for the unroofing history of the Bitterroot metamorphic core complex, Idaho-Montana. *Geological Society of America Bulletin,* 114**,** 448-461.

Hyndman, D. W. (1981) Controls on source and depth of emplacement of granitic magma. *Geology,* 9**,** 244-249.

Ishihara, S. 1981. The granitiod series and mineralization. In *Economic Geology 75th Anniversary Volume,* ed. B. J. Skinner, 458-484. Society of Economic Geologists.

Jaeger, J. C. & N. G. W. Cook. 1969. *Fundamentals of Rock Mechanics*. London: Methuen.

Janecke, S. U. & J. J. Blankenau (2003) Extension folds associated with Paleogene detachment faults in SE part of the Salmon Basin. *Northwest Geology,* 32**,** 51-73.

Janecke, S. U., C. J. Vandenburg & J. J. Blankenau (1998) Geometry, mechanisms and significance of extensional folds from examples in the Rocky Mountain Basin and Range province, USA. *Journal of Structural Geology,* 20**,** 841-856.

Jebrak, M. (1997) Hydrothermal breccias in vein-type ore deposits: A review of mechanisms, morphology and size distribution. *Ore Geology Reviews,* 12**,** 111-134.

Kalakay, T. J., B. E. John & D. R. Lageson (2001) Fault-controlled pluton emplacement in the Sevier fold-and-thrust belt of Southwest Montana, USA. *Journal of Structural Geology,* 23**,** 1151-1165.

Knopf, A. 1950a. The Marysville granodiorite stock, Montana. 834-844. American Mineralogist: Mineralogical Society of America, Washington, DC, United States (USA).

--- (1950b) The Marysville granodiorite stock, Montana. 35**,** 834-844.

Kulik, D. M. & C. J. Schmidt (1988) Region of overlap and styles of interaction of Cordilleran thrust belt and Rocky Mountain foreland. *Geological Society of America Memoir,* 171**,** 75-98.

Lageson, D. R. & M. C. Stickney. 2000. Seismotectonics of Northwest Montana, USA. In *Montana/Alberts Thrust Belt and Adjacent Foreland,* ed. R. A. a. J. Schalla, E.H., 109-126. Billings: Montana Geological Society.

Lowell, J. D. & J. M. Guilbert (1970) Lateral and vertical alteration-mineralization zoning in porphyry copper ore deposits. *Economic Geology,* 65**,** 373-408.

Markey, R. J., J. L. Hannah, J. W. Morgan & H. J. Stein (2003) A double spike for osmium analysis of highly radiogenic samples. *Chemical Geology,* 200**,** 395-406.

Markey, R. J., H. J. Stein & J. W. Morgan (1998) Highly precise Re-Os dating of molybdenite using alkaline fusion and NTIMS. *Talanta,* 45**,** 935-946.

McCay, E. J. 1978. Preliminary geologic map and coal sections, King Mountain Quadrangle, Rosebud and Powder River counties, Montana. Miscellaneous Field Studies Map - U. S. Geological Survey, Report: MF-0817.

McMechan, R. D. & R. A. Price. 1984. Crustal extension and thinning in a foreland thrust and fold belt, southern Canadian Rockies. In *The Geological Society of America, 97th annual meeting*. Reno, NV.

Mohr, O. (1900) Welche Umstände bedingen die Elastitätsgrenze und den Bruch eines Materials? *Zeitschrift de Vereins Deutscher,* 44**,** 1572-1577.

O'Neill, J. M., J. D. Lonn, D. R. Lageson & M. J. Kunk (2004) Early Tertiary Anaconda Metamorphic Core Complex, southwestern Montana. *Canadian Journal of Earth Sciences,* 41**,** 63-72.

Orife, T. & R. J. Lisle (2006) Assessing the Statistical Significance of Paleostress Estimates: Simulations using Random Fault-slips. *Journal of Structural Geology,* 28**,** 952-956.

Petefish, D. M. 1975. Metamorphism in the Marysville geothermal area, Marysville, Montana. 46. Dallas, TX: Southern Methodist University.

Radtke, A. S., R. O. Rye & F. W. Dickson (1980) Geology and stable isotope studies of the Carlin gold deposit, Nevada. *Economic Geology,* 75**,** 269-278.

Ramsay, J. & M. Huber. 1987. *The Techniques of Modern Structural Geology: Folds and Fractures*. London: Acad. Press.

Ranalli, G. & Z. M. Yin (1990) Critical stress difference and orientation of faults in rocks with strength anisotropies: the two-dimensional case. *Journal of Structural Geology,* 12**,** 1067-1071.

Rice, J. (1977) Progressive Metamorphism of Impure Dolomitic Limeston in the Marysville Aureole, Montana. *American Journal of Science,* 277**,** 1-24.

Ross, C. P., B. A. L. Skipp & R. Rezak. 1963. The Belt series in Montana. 122 pp. U. S. Geological Survey Professional Paper.

Ross, G., R. Parrish & D. Winston (1992) Provenance and U-Pb geochronology of the Mesoproterozoic Belt Supergroup (northwestern United States); implications for age of deposition and pre-Panthalassa plate reconstructions. *Earth and Planetary Science Letters,* 113**,** 57-76.

Ross, G. & M. Villeneuve (2003) Provenance of the Mesoproterozoic (1.45 Ga) Belt Basin (western North America); another piece in the pre-Rodinia paleogeographic puzzle. *Geological Society of America Bulletin,* 115**,** 1191-1217.

Rostad, O. H. (1978) K-Ar dates for mineralization in the White Cloud-Cannivan porphyry molybdenum belt of Idaho and Montana; discussion. *Economic Geology,* 73**,** 1366-1368.

Sears, J. W. & M. S. Hendrix. 2004. Lewis and Clark line and the rotational origin of the Alberta and Helena Salients, North American Cordillera. 173-186. Special Paper - Geological Society of America: Geological society of America.

Sears, J. W., M. S. Hendrix, B. Webb & D. Archibald. 1998. Constraints on deformation of the Northern Rocky Mountain fold-thrust belt in Montana from 39Ar/40Ar geochronology of andesitic sills. In *American Association of Petroleum Geologists 1998 annual meeting*. Salt Lake City, UT.

Sears, J. W., K. MacDonald & J. Lonn. 2010. Lewis and Clark Line, Montana: Tectonic evolution of a crustal-scale flower structure in the Rocky Mountains. In *Through the Generations: Geologic and Anthropogenic Field Excursions in the Rocky Mountains from Modern to Ancient: Geological Society of America Field Guide 18,* eds. L. A. Morgan & S. L. Quane, 1-20.

Shirey, R. B. & R. J. Walker (1995) Carius-tube digestion for low-blank Re-Os analysis. *Analytical Chemistry,* 34**,** 2136-2141.

Sillitoe, R. H. 1991. Intrusion-related gold deposits. In *Gold Metallogeny and Exploration,* ed. R. P. Foster. Glasgow, United Kingdom: Blackie and Son.

--- (1993) Epithermal Modeals: Genetic Types, Geometrical Controls, and Shallow Features. *Geological Association of Canada Special Paper,* 40**,** 403-417.

--- (2000) Gold-Rich Porphyry Deposits: Descriptive and Genetic Models and Their Role in Exploration and Discovery. *SEG Reviews,* 13**,** 315-345.

Sillitoe, R. H. (2008) Major Gold Deposits and Belts of the North and South American Cordillera: Distribution, Tectonomagmatic Settings, and Metallogenic Considerations. *Economic Geology,* 103**,** 663-687.

Sillitoe, R. H. & J. W. Hedenquist. 2003. Linkages between Volcanotectonic Settings, Ore-Fluid Compositions, and Epithermal Precious Metal Deposits. In *Special Publication 10,* eds. S. F. Simmons & I. Graham, 315-343. Society of Economic Geologists.

Singer, D. A., V. I. Berger & B. C. Moring (2008) Porphyry Copper Deposits of the World: Database and Grade and Tonnage Models. *USGS Open-file Report,* 2008-1155**,** 1-45.

Smithson, S. B. & R. A. Johnson. 1989. Crustal structure of the Western U.S. based on reflection seismology. In *Geophysical framework of the continental United States,* eds. L. C. Parkiser & W. D. Mooney, 577-612. Boulder, Colorado: Geological Society of America Memoir.

Smoliar, M. I., R. J. Walker & J. W. Morgan (1996) Re-Os ages of group IIA, IIIA, IVA and IVB iron meteorites. *Science,* 271**,** 1099-1102.

Stein, H. J. & B. Bingen. 2002. 1.05-1.01 Ga Sveconorwegian metamorphism and deformation of the supracrustal sequence at Saesvatn, south Norway: Re-Os dating of Cu-Mo mineral occurrences. In *The timing and location of Major Ore deposits in an evolving orogen,* eds. D. Blundell, F. Neubauer & A. von Quadt, 319-335. Geol Soc Lond Spec Publ.

Stein, H. J., J. L. Hannah, A. Zimmerman, R. Markey, S. C. Sarkar & A. B. Pal (2004) A 2.5 Ga porphyry Cu-Mo-Au deposit at Malanjkhand, central India: implications for Late Archaean continental assembly. *Precambrain Res,* 134**,** 189-226.

Stein, H. J., R. J. Markey, J. W. Morgan, A. Du & Y. Sun (1997) Highly precise and accurate Re-Os ages for molybdenite from the East Qinling molybdenum belt, Shaanxi province, Chine. *Economic Geology,* 92**,** 827-835.

Stein, H. J., R. J. Markey, J. W. Morgan, J. L. Hannah & A. Schersten (2001) The remarkable Re-Os chronometer in molybdenite; how and why it works. *Terra Nova,* 13**,** 479-486.

Stein, H. J., A. Scherstén, J. Hannah & R. Markey (2003) Sub-grain scale decoupling of Re and ^{187}Os and assessment of laser ablation ICP-MS spot dating in molybdenite. *Geochim Cosmochim Acta,* 67**,** 3673-3686.

Thompson, J. F. H., R. H. Sillitoe, T. Baker, J. R. Lang & J. K. Mortensen (1999) Intrusion-related gold deposits associated with tungsten-tin provinces. *Mineralium Deposita,* 34**,** 323-334.

Tosdal, R. M. & J. P. Richards. 2001. Magmatic and structural controls on the development of porphyry Cu+ or -Mo+ or -Au deposits. In *Reviews in Economic Geology,* eds. J. P. Richards & R. M. Tosdal, 157-181. Society of Economic Geologists, Boulder, CO.

Walker, G. E. 1992a. Geology and History of the Marysville Mining District and The Drumlummon Mine, Lewis and Clark County, Montana. Montana Bureau of Mines and Geology.

---. 1992b. Geology and History of the Marysville Mining District and The Drumlummon Mine, Lewis and Clark County, Montana. Montana Bureau of Mines and Geology.

Wallace, C. A., D. J. Lidke & R. G. Schmidt (1990) Faults of the central part of the Lewis and Clark Line and fragmentation of the Late Cretaceous foreland basin in west-central Montana. *Geological Society of America Bulletin,* 102**,** 1021-1037.

Wallace, R. E. (1951) Geometry of Shearing Stress and Relation to Faulting. *Journal of Geology,* 59**,** 118-130.

Ward, P. L. 1995. Subduction cycles under western North America during the Mesozoic and Cenozoic eras. In *Jurassic Magmatism and Tectonics of the North American Cordillera,* eds. D. M. Miller & C. Busby, 1-46.

Wernicke, B. 1992. Cenozoic extensional tectonics of the U.S. Cordillera. In *The Cordilleran Orogen: Conterminous U.S.,* eds. B. C. Burchfiel, P. W. Lipman & M. L. Zoback, 553-581. The Geological Society of America.

Žalohar, J. & M. Vrabec (2007) Paleostress analysis of heterogeneous fault-slip data: The Gauss method. *Journal of Structural Geology,* 29**,** 1798-1810.

APPENDICES

APPENDIX A

40AR/39AR GEOCHRONOLOGY RESULTS FOR SAMPLES NEAR THE DRUMLUMMON MINE

DVD available upon request. To request DVD copies contact your local public or university library to place an interlibrary loan request to Montana State University. For questions call (406) 994-3161.

APPENDIX B

ICAL MSU SPECTRUM REPORT

DVD available upon request. To request DVD copies contact your local public or university library to place an interlibrary loan request to Montana State University. For questions call (406) 994-3161.

APPENDIX C

MARYSVILLE DISTRICT FRACTURE DATA

DVD available upon request. To request DVD copies contact your local public or university library to place an interlibrary loan request to Montana State University. For questions call (406) 994-3161.

APPENDIX D

BALD BUTTE OUTCROP DATA

DVD available upon request. To request DVD copies contact your local public or university library to place an interlibrary loan request to Montana State University. For questions call (406) 994-3161.

APPENDIX E

DATA RECORDED AT THE EXPLORATION PIT AT BALD BUTTE

Vein and fault data collected from the exploration pit at Bald Butte. (A) Selected veins mapped during September, 2008. Blue symbols show saccharoidal quartz veins with or without molybdenite. Red symbols show quartz and clay veins. (B) Schematic representation of kinematics of vein sets and faults identified in the exploration pit. (Mapping by Gearity and Childs, 2008).

DVD available upon request. To request DVD copies contact your local public or university library to place an interlibrary loan request to Montana State University. For questions call (406) 994-3161.

APPENDIX F

PLATE A

DVD available upon request. To request DVD copies contact your local public or university library to place an interlibrary loan request to Montana State University. For questions call (406) 994-3161.